

Low-grade prehnite-pumpellyite facies metamorphism and metasomatism in basement rocks adjacent to the Permian Oslo rift: The importance of displacive reactions

Håkon Austrheim¹ | Ane K. Engvik²  | Morgan Ganerød² |
Kristina G. Dunkel¹  | Mari Roen Velo¹

¹Physics of Geological Processes (PGP),
The Njord Centre, Department of
Geosciences, University of Oslo, Oslo,
Norway

²Geological Survey of Norway,
Trondheim, Norway

Correspondence

Håkon Austrheim, Physics of Geological
Processes (PGP), The Njord Centre,
Department of Geosciences, University of
Oslo, PO Box 1048, N-0316 Oslo, Norway.
Email: h.o.austrheim@geo.uio.no

Funding information

Alexander von Humboldt-Stiftung;
Humboldt Prize

Handling Editor: Dr. Katy Evans

Abstract

The Kongsberg and Bamble lithotectonic domains of SE-Norway are known as classical Precambrian high-grade metamorphic terrains. The area has undergone extensive metasomatism with formation of albitites and scapolite-rich rocks and numbers of previously economically important deposits including the Kongsberg Silver and the Modum Cobalt mines. We demonstrate here that the central part of the Bamble lithotectonic domain (Kragerø area) has locally developed low-grade metamorphic minerals (prehnite, pumpellyite, analcime, stilpnomelane and thomsonite) belonging to the prehnite-pumpellyite and zeolite facies. Structurally, the low-grade minerals occur as fracture fills, in the alteration selvages around fractures where the rock is albitized, and along shear zones and cataclastic zones. The fracture fill and the alteration selvages vary from millimetres scale to 1 m in thickness. The fractures with low-grade minerals are part of larger fracture systems. The low-grade minerals typically formed by both displacive (swelling) and replacive reactions and in a combination of these. Prehnite together with albite, K-feldspar, quartz, epidote and hydrogarnet form lenses along (001) faces in biotite and chlorite leading to bending of the sheet silicates through a displacive reaction mechanism. Numerous replacement reactions including the earlier minerals as well as the low-grade minerals occur. As albite, K-feldspar, talc, quartz, actinolite, titanite, calcite and hydrogrossular form in the same veins and in the same biotite grain as the classical low-grade minerals, they probably belong to the low-grade assemblage and some of the albitization in the region presumably occurred at low-grade conditions. Alteration of olivine (Fo69) at low-grade conditions results in the formation of clay minerals including ferroan saponite. Reconnaissance studies at the east (Ideford lithotectonic domain) and the northwest (Kongsberg lithotectonic domain) sides of the Oslo rift together with reports of low-grade assemblages in south-western Sweden along the continuation of the rift into Skagerrak suggest that the low grade assembles

This is an open access article under the terms of the [Creative Commons Attribution-NonCommercial](https://creativecommons.org/licenses/by-nc/4.0/) License, which permits use, distribution and reproduction in any medium, provided the original work is properly cited and is not used for commercial purposes.

© 2022 The Authors. *Journal of Metamorphic Geology* published by John Wiley & Sons Ltd.

occur in rocks adjacent to the Oslo rift along its full extent. Ar-Ar dating of K-feldspar from the low-grade assemblages gave an age of 265.2 ± 0.4 Ma (MSWD = 0.514 and $P = 0.766$), suggesting that the low-grade metamorphism and some of the metasomatism is induced by fluids and heat from the magmatic activity of the Permian Oslo rift, which requires transport of fluid over distances of several kilometres. The metamorphic conditions are constrained by stability fields of prehnite, pumpellyite and analcime to be less than 250°C and at a pressure less than 5 kbars. The displacive reactions created microfractures and porosity in the adjacent minerals that enhance fluid flow and low-grade mineral formation on a local scale. On a thin section scale, the displacive growth of albite in biotite results in a local volume increase of several 100%. Whether the opening of the larger, horizontally oriented fracture systems needed to transport the fluid over a distance of several kilometres was also the result of displacive reactions remains unknown. The low-grade metamorphism and metasomatism formed in the shoulder of the Oslo rift and may have contributed to its uplift.

KEYWORDS

albitization, displacive reactions, Permian Oslo rift shoulder, prehnite-pumpellyite facies, replacement reactions

1 | INTRODUCTION

The type environment for low-grade metamorphism, that is, zeolite and prehnite-pumpellyite facies metamorphism, is burial of volcanoclastic rocks as outlined in the classical papers by Coombs and co-workers from New Zealand (Coombs, 1954, 1960; Coombs et al., 1959). Subsequent work has shown that low-grade minerals may form in a variety of other rock types and tectonic settings. Low-grade minerals occur in subduction settings (Kamimura et al., 2012), at the ocean floor (Spooner & Fyfe, 1973), in island arcs (Miron et al., 2012), in gneiss terrains (Morad et al., 2011; Möller & Söderlund, 1997; Zeck, 1971), as veins in metadolerite (Sansone & Rizzo, 2012) and as veins in amphibolite facies basement gneisses (Weisenberg & Bucher, 2011). Already Eskola (1939) recognized that these minerals formed by hydrothermal processes and therefore questioned if the zeolite and prehnite-pumpellyite facies should indeed be referred to as metamorphic facies. The fluid-rich environments characteristic for low-grade metamorphism may also lead to metasomatism, particularly albitization (Miron et al., 2012) and ore-forming processes (Alonso-Azcarate et al., 1999; White et al., 2014). Low-grade metamorphism grades with decreasing temperature into diagenetic processes (Frey & Robinson, 2009). Thus, the processes active at low-grade metamorphism are of interest to a broader audience of sedimentologists and

petroleum geologists. Combs (1954) was the first to recognize the importance of albitization during burial of sediments. Large-scale hydrothermal alteration including albitization occurs in sedimentary basins and may modify reservoir-quality (Mansurbeg et al., 2020; Saigal et al., 1988). Well-constrained conditions for albitization were given by Boles (1982) who reported active albitization in the Gulf Coast Tertiary at temperatures varying from 110 to 120°C and at a depth between 2500 to 2870 m.

Although the Kongsberg and Bamble lithotectonic domains in Southern Norway are known as classical high-grade terranes (Engvik et al., 2016; Nijland et al., 2014; Touret, 1971), low-grade minerals have been reported to form a number of localities in both domains. Field and Rodwell (1968) reported an occurrence of prehnite in the high-grade metamorphic sequence from the area between Risør and Tvedestrand. Dahlgren et al. (1993) describe prehnite, albite and laumontite from hydrothermal carbonate breccias from the Kragerø area. Nijland et al. (1993) ascribe the low-grade minerals from Froland to retrogressive metamorphism. Visser (1993) and Nijland et al. (1994) report F-bearing hydrogarnets intergrown with prehnite, pumpellyite, epidote and chlorite along biotite cleavage planes from Blengsvatn and Arendal area, both in the Bamble domain. Stilpnomelane has been described from the Modum area (Munz et al., 2002) and the Valberg quarry (Nordrum et al., 2000). Recent investigations (Austrheim

et al., 2008; Engvik et al., 2014; Jamtveit & Austrheim, 2010; Putnis & Austrheim, 2010) have shown that the minerals prehnite, pumpellyite and analcime are present in several localities around Kragerø. In this paper, we present a more comprehensive study of the low-grade parageneses of the area, including their regional distribution, their textural and structural settings, and their age. Our investigation is focused on the Kragerø area in Bamble (9 localities), but we also include data (Table 1) from two localities in the Kongsberg domain and one locality in the Idefjord lithotectonic domain. We conclude that the low-grade minerals, although localized to fluid pathways, occur on a regional scale and that the area has therefore undergone a low-grade prehnite-pumpellyite facies event, as defined by Coombs et al. (1976). The introduction of fluid into a nominally impermeable rock like gabbro and gneiss calls upon a mechanism that can open the rock for fluid flow. Either this may be tectonic stresses or reaction enhanced fracturing possibly combined with dissolution and reprecipitation (Putnis, 2002). We document here that low-grade assemblages in the Kragerø area are characterized by displacive textures caused by growth of albite and the low-grade minerals in biotite and other sheet silicates, locally leading to fragmentation of the surrounding minerals, suggesting that reaction enhanced fragmentation is important. We also note that replacement textures typical for a dissolution-precipitation mechanism are common in the studied rocks. We further find that the hydrothermal activity leading to the low-grade metamorphism and associated metasomatism was driven by heat and fluid from the magmatic activity in the Permian Oslo rift.

2 | GEOLOGICAL SETTING

The Oslo rift extends from the Sorgenfrei-Tornquist Zone to Lake Mjøsa over a total length of 400 km (Neumann et al., 1992) and is part of an intricate system of rifts or grabens that developed in Northwest Europe from the Carboniferous to the Cretaceous (Ziegler, 1978). The northern part of the Oslo rift, the Oslo graben, is exposed on land and continues offshore as the Skagerrak graben (Ro et al., 1990).

The Oslo rift is bounded in the west by the Kongsberg (north) and Bamble (south) lithotectonic domains and in the east by the Idefjorden lithotectonic domain (Figure 1). The Bamble lithotectonic domain refers to a 30 km wide zone of dominantly Precambrian rocks that extends from Kristiansand in the south for 150 km northward where it terminates towards the Oslo rift. The Kongsberg lithotectonic domain to the north of the rift is interpreted to be a continuation of the Bamble domain

(Bingen et al., 2005; Bugge, 1936), although this has been questioned by Andersen (2005). The Bamble domain is known for its high-grade granulite facies metamorphism, including the first mapped orthopyroxene isograd (Touret, 1971), and for being extensively metasomatized. Metasomatism led to the formation of albitite bodies (Engvik et al., 2008, 2014, 2018), scapolite-rich rocks (Engvik et al., 2009, 2011; Lieftink et al., 1993), orthoamphibole-cordierite rocks (Engvik & Austrheim (2010); Hövelmann et al., 2014) and nodular gneisses (Nijland et al., 2014). Similar metasomatic rocks are also present in the Modum region of the Kongsberg domain. The metasomatism in both domains also resulted in the formation of a number of previously economically important deposits. These include the Ødegården apatite and rutile deposits, the Langøya Fe-mineralization that for a long period (17th to midst of the 19th century) provided iron for the smelters in Oslo (Kristiania), the famous Kongsberg silver mineralization and the Modum cobalt ore. The tectonic setting in which these rocks formed and evolved is poorly known and so is the relationship between the metamorphic and metasomatic events although there is a consensus that they are related to the Sveconorwegian orogeny. This is based mainly on U–Pb ages of rutile and titanite and Rb–Sr ages from albitized rock reported by Engvik et al. (2011, 2017). The ages reported range from 1084 to 1104 Ma and are interpreted to date the albitization.

The Kragerø region, where most of our data is collected, is located in the centre of the Bamble domain and is characterized by a number of gabbros, including the Langøy troctolite gabbro (Vogt, 1910), Valberg gabbro, Ødegården metagabbro (Brögger, 1935) and Ringsjø gabbro body. The gabbros are variably amphibolitised, scapolitized and albitized. The pristine parts are medium-grained dark rocks that display corona textures where olivine is surrounded by an inner rim of orthopyroxene and an outer rim of intergrown spinel and amphibole. The gabbros were hydrated (amphibolitized) before they experienced Cl-metasomatism, leading to the formation of scapolite (Engvik et al., 2011; Kusebauch, John, Barnes, et al., 2015; Kusebauch, John, Whitehouse, et al., 2015; Lieftink et al., 1993). The product is a scapolite-metagabbro (also called ødegårdite; Brögger, 1935) that consists of scapolite, phlogopite, amphibole, rutile and apatite.

3 | METHODS

The samples have been studied with a range of analytical techniques (see below) including extensive use of optical microscopy. Biotite varies in Mg/Fe ratio and

TABLE 1 Mineralogy and textures of low-grade assemblages, around the Oslo rift with focus on the Kragerø region, S-E-Norway

| Sample | Locality | E-UTM32 | N-UTM32 | Rock type | Primary minerals | Low-grade minerals | Textures | Reference |
|--------------|----------------|---------|---------|-----------------------------------|---------------------------|-----------------------|----------------|-----------|
| Ri01-09 | Ringsjø | 530200 | 6534900 | Metagabbro | Scp, Bt, Amp | Prh, Pmp, Ab | | This work |
| AE113 | Ringsjø | 530200 | 6534900 | Metagabbro | Amp, Pl, Rt, Bt | Prh, Ab | S1, S2 | This work |
| AE69 | Ringsjø | 530200 | 6534900 | Oam-Crd gneiss | Oam, Cdr, Qz, Rt | Penitized | | This work |
| Ri4B | Ringsjø | 530200 | 6534900 | Scp-metagabbro | Scp, Amp, Bt, Ru, Ap | Ab | R2, S1 | This work |
| Ri05B | Ringsjø | 530200 | 6534900 | Scp-metagabbro | Scp, Amp, Bt, Ru, Ap | Ab | R3, S1 | This work |
| Mv13.35 | Kil Brygge | 517600 | 6528300 | Scp-metagabbro | Amp, Bt, Pl, Scp, Ep | Prh, Anl, Cal, Ttn | S5 | This work |
| Mv13.29 | Ødegården verk | 532000 | 6535700 | Pyroxenite | Opx, Bt | Tlc | R5 | This work |
| Mv13.31 | Ødegården verk | 532000 | 6535700 | Phlogopite layer | Bt, Opx | Tlc, Ab | S1, R5 | This work |
| Mv13.27 | Valberg-quarry | 524100 | 6527100 | Metagabbro, albitized | Ab, Amp, Prh, Ttn | Prh | | This work |
| 1Ø17.30 | Ødegården verk | 532000 | 6535700 | Metagabbro, albitized | Pl, Ap, Chl, Rt, Cal, Ttn | Pmp | | This work |
| Mv13.38 | Lindvikkollen | 521400 | 6525300 | Scp-metagabbro | Bt, Amp, Plag | Ser | R4, R6 | This work |
| Val-Gp2-3-14 | Valberg-quarry | 524100 | 6527100 | Scp-metagabbro | Scp, Bt, Amp | | S1, S2 | This work |
| Val Gp4-4-14 | Valberg-quarry | 524100 | 6527100 | Metagabbro | Pl, Amp, Bt | Ab | S1 | This work |
| Val-A-6-1 | Valberg-quarry | 524100 | 6527100 | Prehnite vein, in metagabbro | | Prh, Cal, Ab, Rt | V2 | This work |
| Val-A-6-2 | Valberg-quarry | 524100 | 6527100 | Alteration selvage, in metagabbro | | Prh, Cal, Ab, Rt, Chl | | This work |
| Val-A-6-5 | Valberg-quarry | 524100 | 6527100 | Scp-metagabbro | Bt, Amp, Scp | Prh, Cal, Ab | S1 | This work |
| Val-Gp3-3-14 | Valberg-quarry | 524100 | 6527100 | Scp-metagabbro | Ep | | | This work |
| DH2-b | Valberg-quarry | 524100 | 6527100 | Bt-rich layer, in metagabbro | Bt | Prh, Pmp, Hgr | S1, S2, S4 | This work |
| BAM2-12 | Valberg-quarry | 524100 | 6527100 | Scp-metagabbro | Scp, Bt, Amp | Alb, Cal, Ttn | R1, S1, V2 | This work |
| Val-Gp2-14-2 | Valberg-quarry | 524100 | 6527100 | Metagabbro | Ol, Pl, Opx, Amp | Prh, Pmp, Thm, Ab | V1, V2, V4, V6 | This work |
| B-2-1,M | Valberg-quarry | 524100 | 6527100 | Scp-metagabbro | Scp, Bt, Amp | Ab, Cal, Ttn | S1 | This work |
| ATI-KS | Åtangen | 520000 | 6525300 | Scp-metagabbro | Amp, Scp | Anl, Cal | V5 | This work |
| AE141 | Åtangen | 520100 | 6525900 | Oam-bearing amphibolite | Oam, Pl | Chl, Cal | S8, R5 | This work |
| La07-09 | Langøy west | 528230 | 6529580 | Brecciated Scp-metagabbro | Scp, Amp, Fe-Ti oxides | Anl, Cal, Chl | R6 | This work |

(Continues)

TABLE 1 (Continued)

| Sample | Locality | E-UTM32 | N-UTM32 | Rock type | Primary minerals | Low-grade minerals | Textures | Reference |
|---------|--|---------|---------|--------------------------------------|------------------------------------|-----------------------------|------------|-----------------------------|
| BG94 1A | Parrisholmen | 533800 | 6528000 | Grt-amphibolite | Grt, Pl, Bt, Qz, Amp, Fe-Ti oxides | Prh | S2, R4 | This work |
| JL1 | Jomfrulund | 535200 | 6526200 | Banded gneiss | Amp, Fsp, Bt, Ttn | Prh, Pmp, Ab, Act, Chl | S2, S7 | This work |
| AE126B | Valle | 532200 | 6532600 | Sill-nodular gneiss | Qz, Wm, Bt, Sil, Tur | Kln | V3 | This work |
| AE131 | Valle | 532200 | 6532600 | Sill-nodular gneiss with mafic layer | Pl, Cpx, Bt, Qz, Wm, Ttn | Pmp | R4 | This work |
| FOL1-14 | Kjøvangen, Vestby | 594100 | 6601100 | Amphibolite | Amp, Pl, Bt | Prh, Ab, Act, Chl | S2, V2, R7 | This work |
| FOL3-14 | Kjøvangen, Vestby | 594100 | 6601100 | Amphibolite | Amp, Pl, Bt | Chl, Cal | S2, S1, R7 | This work |
| GAI | Gampehue, Modum | 544900 | 6649000 | Metagabbro | Amp, Pl, Ilm, Grt | Pre, Pmp, Ab, Act, Chl, Ttn | V1, V2 | Austrheim et al., 2008 |
| BLA-13 | Sarasåsen, Ringerike | 560100 | 6665400 | Coronitic troctolite | Ol, Pl, Opx, Amp | Pmp | V4 | Larsen, 2014 |
| BLA-16 | Sarasåsen, Ringerike | 560100 | 6665400 | Coronitic troctolite | Cpx, Amp | Prh, Srp | V2 | Larsen, 2014 |
| | Risør/Tvedestrand | | | | | Prh | | Field and Rodwell (1968) |
| | Kleggåsen, Frøland | | | | | Prh, Pmp, Tur | S2, S5 | Nijland et al. (1993) |
| | Blengsvatn | | | | | F-Hgr, Prh, Pmp | | Visser (1993) |
| | Arendal | | | | | F-Hgr, Prh, Pmp | | Nijland et al. (1994) |
| | Modum | | | | | Stp | | Munz et al. (2002) |
| | Valberg-quarry | | | Scp-metagabbro | | Stp | | Nordrum et al. (2000) |
| | Kragerø area | | | Permian dykes | | Prh, Pmp, Stp | | Sauter et al. (1983) |
| | Kragerø area | | | Carbonate breccias | | Prh, Lmt | | Dahlgren et al. (1993) |
| | From Gøteborg, Sweden, to the Norwegian border | | | Qtz-fsp-gneiss & granitoid | | Prh, Pmp | S2, S3 | Zeck (1971) |
| | Gällared, Sweden | | | Granitic dyke | | Pmp | | Möller and Soderlund (1997) |

Note: Abbreviations after Whitney and Evans (2010).

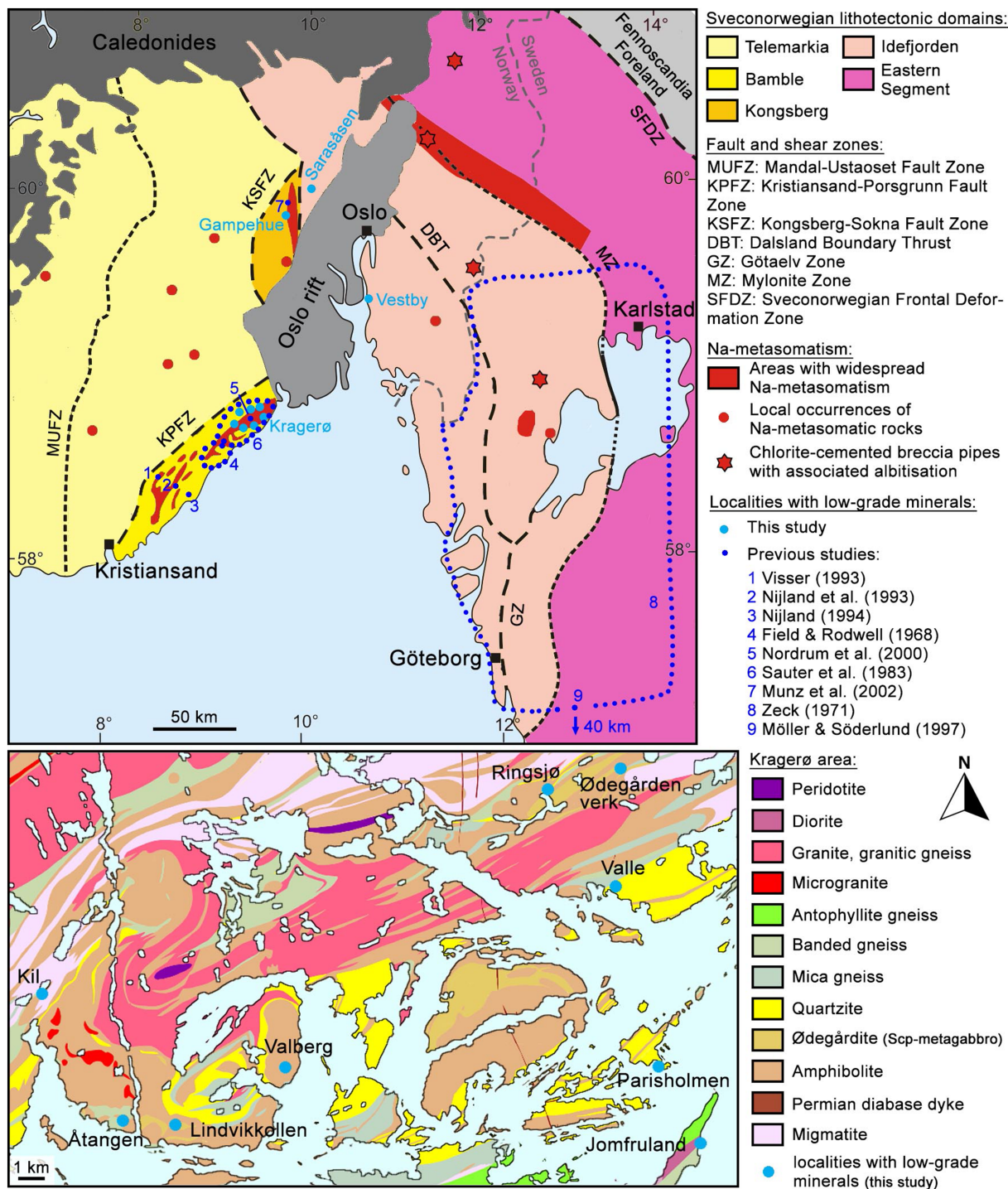


FIGURE 1 Maps showing the localities with low-grade minerals around the Oslo rift. The upper map (after Bingen et al. (2008) and Engvik et al. (2014)) depicts the Sveconorwegian lithotectonic domains around the Oslo rift. The localities of Na-metasomatism (albitisation) are given in red (after Engvik et al., 2014). Localities from which low-grade minerals have been described previously are marked in dark blue; localities sampled for the current study in light blue. A more detailed geological map of the Kragerø area, where most of the data for this study was collected, is given in the bottom map (geological units from the geological survey of Norway). Note the thin Permian dykes extending from the rift into this part of the Bamble lithotectonic domain.

classifies as phlogopite in some samples. Because we did not systematically measure every biotite grain, we do not differentiate between different biotite endmembers in the text.

3.1 | Electron microprobe techniques

Mineral compositions were obtained by wavelength dispersive analysis using a Cameca SX100 electron

microprobe at Department of Geosciences, University of Oslo. Natural minerals and synthetic phases were used as standards. The accelerating voltage was 15 kV, and the beam current varied between 10 and 15 nA. Analcime and albite were analysed by a defocused beam to reduce evaporation. The counting time was 10 s on both peak and background. Data reduction was carried out with the Cameca PAP software package.

3.2 | Scanning electron microscopy

BSE images were also acquired by a Hitachi SU5000 also located at the Department of Geosciences, University of Oslo. We used the EDX detector extensively to identify the fine-grained minerals.

3.3 | Pseudosections

The stability fields of indicator minerals (prehnite, pumpeyite and analcime) were calculated with *Perple_X* (Connolly, 2005), using the thermodynamic database *hp02.dat* (Holland & Powell, 1998, as revised by the authors), under fluid (pure H₂O, and H₂O/CO₂) conditions. Only pure endmembers were considered.

3.4 | Estimation of volume increase by displacive reactions

The volume increase caused by displacive growth of albite in biotite listed in Table 2 was calculated based on BSE. We selected areas such as in Figure 5b, where albite has grown between sheets of biotite. The amount of biotite is assumed to be the original volume, and the amount of albite the added volume. The area fractions of each mineral were calculated based on the range of greyscale values they represent. Biotite is locally replaced by chlorite in which case biotite participates in the reaction. We avoided such areas for our estimates, but nevertheless recognize that our estimates are maximum values. The growth of albite on cleavage planes of biotite requires mobility of Al, an element commonly assumed to be immobile. High mobility of Al has however been

reported during low-grade hydrothermal metamorphism by Morad et al. (2009).

3.5 | Ar-Ar geochronology

The rock samples were crushed, grounded and subsequently sieved to obtain 180–250 µm fractions. The mineral separates were washed in acetone and deionized water several times and finally handpicked under a stereomicroscope. Mineral grains with coatings or inclusions were avoided. The samples were packed in aluminium capsules together with the Taylor Creek Rhyolite (TCR) flux monitor standard along with pure (zero age) K₂SO₄ and CaF₂ salts. The sample were irradiated at IFE (Institutt for Energiteknikk, Kjeller, Norway) for ca. 140 h with a nominal neutron flux of $1.3 \times 10^{13} \text{ n}^* (\text{cm}^{-2}\text{s}^{-1})$. The correction factors for the production of isotopes from Ca were determined to be $(^{39}\text{Ar}/^{37}\text{Ar})_{\text{Ca}} = (3.07195 \pm 0.00784) \times 10^{-3}$, $(^{36}\text{Ar}/^{37}\text{Ar})_{\text{Ca}} = (2.9603 \pm 0.026) \times 10^{-4}$ and $(^{40}\text{Ar}/^{39}\text{Ar})_{\text{K}} = (1.3943045 \pm 0.0059335) \times 10^{-1}$ for the production of K (errors quoted at 1σ). The samples were put in a 3.5 mm pit size aluminium sample disk and step heated using a defocused 3.5 mm laser beam with a flat energy spectrum (Photon Machines Fusions 10.6). The extracted gases from the sample cell were expanded into a two-stage low-volume extraction line (ca. 300 cm³), both stages equipped with SAES GP-50 (st101 alloy) getters running cold. They were analysed with an automated MAP 215-50 mass spectrometer in static mode, installed at the Geological Survey of Norway. The peaks were determined during peak hopping for 10 cycles (15 integrations per cycle, 30 integrations on mass ³⁶Ar) on the different masses (^{41–35}Ar) on a Balzers electron multiplier (SEV 217) and regressed back to zero inlet time. Blanks were analysed every third measurement. After blank correction, a correction for mass fractionation, ³⁷Ar and ³⁹Ar decay, and neutron-induced interference reactions produced in the reactor was undertaken using in-house software (AgeMonster written by M. Ganerød). It implements the equations of McDougall and Harrison (1999) and the newly proposed decay constant for ⁴⁰K after Renne et al. (2010). A ⁴⁰Ar/³⁶Ar ratio of 298.56 ± 0.31 from Lee et al. (2006) was used for the atmospheric argon correction and mass

TABLE 2 Volume increase for swelling structures calculated from modal composition of albite and biotite

| Sample | Albite | Biotite | % increase | Comments |
|------------|--------|---------|------------|------------------|
| Ri05B-1B | 83.2 | 16.8 | 595.2 | |
| Val-gp6-20 | 35.1 | 59.3 | 159.2 | Contain 5.6% amp |
| Ri05B-2b | 67 | 33 | 303.0 | |

discrimination calculation (power law). We calculated J-values relative to an age of 28.619 ± 0.036 Ma for the TCR sanidine flux monitor (Renne et al., 2010). We define a plateau according to the following requirements: at least three consecutive steps overlapping at the 95% confidence level (1.96σ) using the strict test:

$$abs(age_n - age_{n+1}) < 1.96 \sqrt{\sigma_n^2 + \sigma_{n+1}^2} \text{ (errors quoted at } 1\sigma \text{)}$$

and mean square of weighted deviates (MSWD) less than the two tailed student T critical test statistics for $n - 1$. Weighted mean ages are calculated by weighting on the inverse of the analytical variance.

4 | OCCURRENCE OF LOW-GRADE MINERALS AROUND THE OLSO RIFT

4.1 | Regional distribution of low-grade minerals

For this contribution, we consider prehnite, pumpellyite, analcime, zeolites, stilpnomelane, kaolinite and hydrogarnet as indicative for low-grade metamorphism. We include hydrogarnet in this list because it forms in equilibrium with the other minerals (see Section 6.1), which are more traditionally considered indicative for low-grade conditions. Epidote and chlorite also locally form together with the low-grade minerals, but because these minerals are so frequently found in higher-grade rocks as well, we do not use them as indicators for low-grade. Albite also occurs in equilibrium with the low-grade minerals but is not used as an index mineral because the origin of albitites is disputed as discussed in Section 10.1.

Table 1 gives an overview of the localities from which low-grade minerals are described here, with the sampled rock types, their primary and secondary mineralogy and their alteration textures. Earlier descriptions of low-grade minerals around the Oslo rift are included as well. Documentation of low-grade minerals is concentrated in the Bamble lithotectonic domain SW of the Oslo rift (Figure 1). This is also where the main focus of this study lies. However, low-grade assemblages were also found in the Kongsberg domain NW of the Oslo rift, and in the northernmost and southernmost parts of the Idefjorden domain.

The samples from the Kragerø area were collected at different distances to the boundary of the Oslo rift (with a distance of ca. 15 km between the westernmost and easternmost samples). There is no systematic change in

paragenesis with sampling locality (Table 1). Neither degree nor type of low-grade alteration increases towards the rift. For example, hydrogarnet is present in the easternmost (Jomfruland) and westernmost samples (Ringsjø).

4.2 | Structural settings of the low-grade minerals

The low-grade minerals are found in veins, which transect the regional foliation at high angles (Figure 2), and in alteration haloes surrounding these veins. The veins are generally millimetres to centimetres thick. The mineralogy of the vein varies with the host rock; however, different vein types can occur in the same host rock.

In mafic rocks, veins containing mainly analcime, prehnite, albite and calcite are common. Analcime and prehnite are typical for scapolite-rich mafic rocks. Some of the analcime veins develop into microbreccias where analcime surrounds fragments of scapolite. Albite and actinolite-calcite-quartz veins may form an echelon pattern and can be traced for tens of meters. Some quartz-actinolite-calcite veins are open. Vugs partly filled with quartz, and calcite crystals are found along the larger fracture zones.

In the more felsic nodular gneiss at Valle, kaolinite-filled veins are found to transect quartz. The low-grade minerals are also found in cataclastic zones and shear zones and seem to follow mica-rich bands.

Some of the veins with low-grade minerals have developed metasomatic haloes with thicknesses varying from micrometres (e.g. albite rims on plagioclase grains) over centimetres (Figure 2b,c) to meters (Figure 2a).

In the following, we describe some vein types and their associated alteration haloes from our main study area in Kragerø in more detail.

5 | LOW-GRADE MINERALS IN THE KRAGERØ AREA: VEINS AND ALTERATION HALOES

5.1 | Ringsjø locality

At the road cuts on the north-western side of lake Ringsjø, scapolite-metagabbro is cut by albite and by actinolite-calcite-quartz veins. The albite veins (Figure 2a) are reddish and contain minor K-feldspar. They are surrounded by green alteration haloes consisting mainly of albite, chlorite and hydrogarnet. Chlorite replaces amphibole, and rutile is replaced by titanite. Displacive textures, as described in Section 6.1, are



FIGURE 2 Metasomatism around veins with low-grade minerals. (a) Field photo showing horizontal fracture set with 50 cm thick alteration selvages from the Ringsjø locality. The fracture system can be followed for more than 100 m on to neighbouring outcrops. (b) Albite vein (pinkish) with a green zone where the scapolite-metagabbro is altered to chlorite and albite with small hydrogarnet. Ringsjø locality. (c) Prehnite vein with a selvage where the scapolite-metagabbro (on the right) is altered to albite and prehnite, Valberg quarry.

concentrated in the green halo but may extend beyond the metasomatic front into the scapolite-metagabbro.

The actinolite-calcite-quartz veins are part of a large-scale vein system (Figure 2b). The alteration haloes surrounding them consist of two zones, an inner red zone and an outer light green zone. In the green zone, the scapolite is replaced by albite and the amphibole is altered to chlorite. In the red zone, albite with a chess-board texture dominates, which is intergrown with K-feldspar. Calcite, Mg-rich chlorite, rutile and apatite occur as well. Small grains of hydrogarnet are present mainly as inclusions in chlorite.

5.2 | Valberg quarry

The scapolite-metagabbro at the Valberg quarry is transected by veins filled with prehnite (and subordnately calcite and albite), varying in width from a few mm to several cm (Figure 2c). The central veins contain 0.5 cm large transparent, fan shaped prehnite crystals radiating perpendicular from the vein boarder. Large calcite crystals (>1 cm across) occur together

with the prehnite in addition to domains of albite. The thicker veins develop a marked, several centimetre thick alteration halo, where the scapolite-metagabbro becomes white due to extensive albitization and the growth of prehnite (Figure 2c). Prehnite and albite are cloudy due to numerous inclusions and pores. In addition to albite and prehnite, chlorite and rutile are present in the white haloes. A sample collected ca. 5 cm away from the vein (Val-A-6-5) contains the relict minerals scapolite, amphibole and biotite. Even this sample, however, which was initially sampled as the wall rock, contains prehnite and calcite.

Albitites similar to the red alteration zones surrounding actinolite-calcite-quartz veins at Ringsjø are also present in the Valberg quarry, where sample Mv13.27 is an albitite with chlorite after biotite together with prehnite, actinolite and titanite.

A less metamorphosed, coronitic gabbro at Valberg locally displays millimetre wide shear fractures arranged en echelon, along which the rock is altered to a low-grade mineralogy including pumpellyite, analcime, thomsonite and prehnite and a clay phase after olivine (see Section 6.3).

6 | TEXTURAL RELATIONSHIPS INVOLVING LOW-GRADE MINERALS

The low-grade minerals occurring in alteration zones surrounding veins in the Kragerø area form in two main textural settings: (1) displacive growth between cleavage faces in sheet silicates (biotite, more rarely chlorite) (Section 6.1) and (2) replacement of pre-existing minerals (Section 6.2). A combination of displacive and replacive reactions also occurs. Particularly, the displacive reactions can cause significant deformation (Section 6.3).

6.1 | Displacement textures

Displacive growth is particularly common in the scapolite-metagabbro, which contains biotite in addition to amphibole, Cl-CO₂-scapolite, minor rutile and variable amounts of apatite. A number of minerals (albite, hydrogarnet, K-feldspar, Fe-oxides, quartz, epidote and calcite) besides the typical low-grade minerals prehnite and pumpellyite form lenses along the cleavage planes of pre-existing minerals (mainly biotite, but also chloritized biotite and amphibole). The growth of minerals inside biotite, for example, results in a bending of the sheet-silicate as illustrated in Figure 3a. In some cases, biotite is folded where schlieren of biotite form both boxfolds and open folds (Figure 3b).

Albite is by far the most common phase to displace biotite (Figure 3a–e). In most cases, it nucleates inside the grain, but it may also start from the rim and form a wedge between (001) faces (Figure 3b). A median line (Figure 3c) within the albite lenses defined by small inclusions (probably titanite) may represent the nucleation line. The albite is fibrous with the long dimension perpendicular to the (001) face of biotite (Figure 3d). In the most well-developed lenses, where the biotite is strongly curved, the albite fibres are also bent as they continue to grow perpendicular to the (001) phase of biotite (Figure 3d).

Several low-grade minerals may occur together displacing the same grain. For example, in sample DH2-b from Valberg, hydrogarnet is found in the same chloritized biotite grains as prehnite and albite, which implies that hydrogarnet is part of the low-grade assemblage (Figure 3e). Similarly, K-Feldspar and prehnite grow together in chloritized biotite from Kil Brygge (Figure 3f).

The modal amount of the minerals grown along the (001) faces in biotite varies strongly. There are single lenses of low-grade minerals with a short axis of 10 µm perpendicular to the (001) plane of biotite. In advanced stages, the amount of low-grade minerals is significant

and domains of albite with a short axis of 50 µm are separate by thin (down to 1 µm) slivers of biotite (Figure 3a,b). The ratio of albite to biotite in such aggregates may be as high as 10:1 (Table 2) but more commonly, a ratio of 5:1 is observed. This implies a volume increase of 500% during the growth of the low-grade minerals, assuming that no dissolution or chloritization, which may change the volume of the remaining biotite, took place.

6.2 | Replacement textures

Replacement is particularly common for amphibole, which is altered to chlorite, titanite and locally calcite (Figure 4a). Chlorite formed by replacement of amphibole can itself be replaced by pumpellyite, actinolite and calcite (Figure 4b). The alteration of amphibole may be erratic and patchy. The reaction products are often porous (Figure 4a,b).

Although biotite typically forms the locus for displacive mineral growth, biotite may also be pseudomorphically replaced by albite with inclusions of titanite. This is the case where single grains of biotite are enclosed by rigid amphibole (Figure 4c). Biotite can also be replaced by prehnite (Figure 4d). Multiple reactions are recorded for biotite as well: In sample AE113, albite is replacing lens-shaped aggregates of prehnite and titanite formed after biotite (Figure 4d). The titanite inclusion from the prehnite remains as inclusions in the albite.

Scapolite is replaced by albite with calcite inclusions (Figure 5). Albite grains with a diameter in excess of 1 cm are present both at Ringsjø and at Valberg (Figure 5a,b). The albite porphyroblasts (single crystals) replace many finer-grained scapolite grains with different crystallographic orientation (Figure 5b). The interphase between the scapolite and the albite with calcite inclusions is sharp (Figure 5c). A Ca-map (Figure 5d) illustrates the concentration of Ca in calcite among the reaction products. Cl is limited to the scapolite; Cl-rich inclusions are apparently absent in the product phases (Figure 5e).

In the Valberg coronitic gabbro, replacement reactions occur along shear fractures (Figure 6a). Plagioclase is altered to analcime, prehnite and thomsonite (Figure 6b). Where the fractures transect olivine (Fo69), it is altered to clay-like substances that change in colour from olive green (close to the vein) to brown close the relict olivine (Figure 6c). Attempts to identify the phases by Raman spectroscopy failed, but the crystallinity of the material was confirmed by well-defined peaks. The stoichiometry (Table S7) suggests that the clay material is a saponite. The alteration occurs in compartments confined by pre-existing serpentine veins (Figures 6c,d).

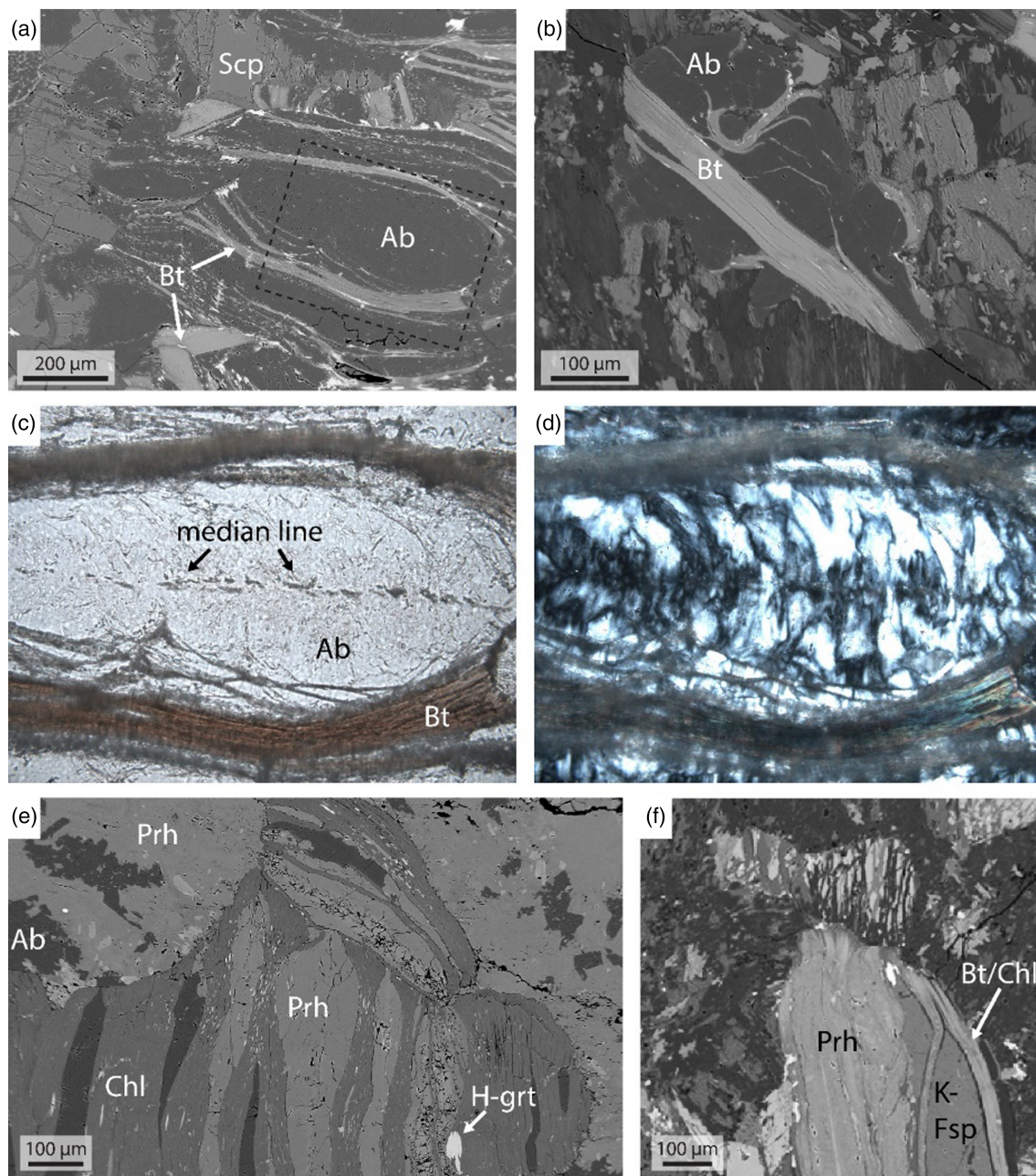


FIGURE 3 Swelling texture caused by displacive growth of low-grade minerals in biotite. (a) BSE image of albite lens surrounded by bent biotite. Fractures filled with chlorite are developed in scapolite grains located left of the albite lens. The fractures may have opened by forces set up by the growing albite lens. The stippled black box gives the location of the optical micrographs in (c) and (d), sample Ri05B, Ringsjø. (b) BSE image showing folding (both open folds and box folds) of biotite by albite growth. Note that this biotite grain is wedged open from its margin. Sample B-2-1 M, Valberg. (c) Photomicrograph in plane-polarized light of the central albite lens shown in (a). A median line defined by small inclusions may represent the nucleation sites of albite. (d) Photomicrograph in cross-polarized light of the same lens as shown in (c). The albite lens consists of sigmoidal fibres that extend out from the median line. Extinction shadows suggest that the albite is strained in accordance with the bending of the biotite. Sample Ri05B, Ringsjø. (e) BSE image showing growth of albite (Ab), prehnite (Prh) and hydrogarnet (H-Grt) inside the same chloritized (chlorite: Chl) biotite grain. Some of the prehnite lenses have a brecciated central part suggesting syn-growth deformation as a consequence of expansion. Sample DH2, Valberg quarry. (f) BSE image showing growth of prehnite and K-feldspar (K-Fsp) in partly chloritized biotite. See Figure S1 for element maps of this area, including information on the surrounding minerals. Sample MV13.35, Kil Brygge

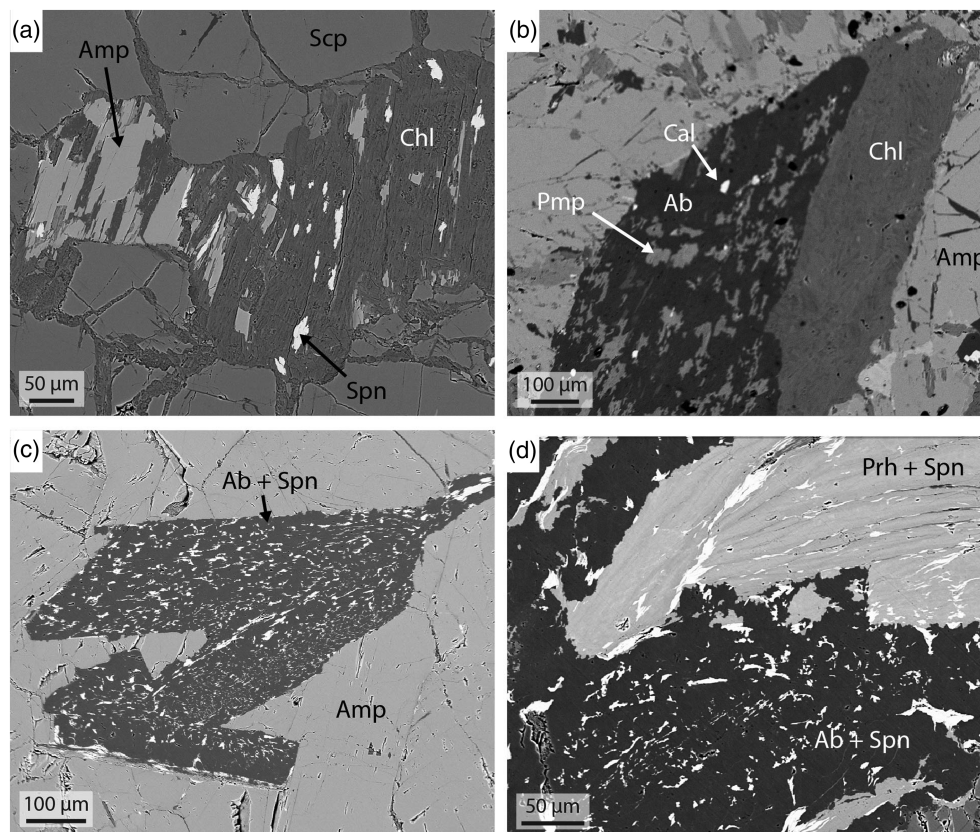


FIGURE 4 Replacement of amphibole and biotite by low-grade minerals. (a) Patchy replacement of amphibole (amp) by chlorite (Chl) and sphene (Spn). Sample Ri04B, Ringsjø. (b) Pseudomorphic replacement of amphibole by chlorite and subsequently replacement of chlorite by albite (Ab), pumpellyite (Pmp) and calcite (Cal). Sample Val-Gp4-1, Valberg. (c) Pseudomorphic replacement of biotite by albite and sphene. No apparent deformation of the surrounding amphibole. Sample AE113, Ringsjø. (d) Biotite has been replaced (Prh) by prehnite and sphene/titanite. The prehnite is subsequently replaced by albite. The sphene inclusions from the prehnite survive the albite replacement and remain as inclusion in albite. Sample AE113, Ringsjø

6.3 | Fractures and porosity associated with the growth of low-grade minerals

Apart from the swelling and bending of the mineral in which the low-grade minerals grow, the displacive reactions also cause deformation of other surrounding minerals (which may lead to enhanced reaction), and of the newly growing minerals themselves.

In scapolite-metagabbros, the 120° cleavage in amphibole is opened, and filled with albite (Figure 7a). Scapolite shows an increased fracture density at the high stress points around biotite being displaced by albite (Figure 7b). At such points, reaction of the scapolite to analcime and calcite is enhanced. Where prehnite displaces and replaces biotite (Figure 7c), the surrounding scapolite contains prehnite-filled veins.

The low-grade minerals may themselves be deformed as demonstrated by displacive prehnite and pumpellyite with fractured cores (Figures 3e and 7d). Newly grown epidote exhibits microfaulting (Figure 7f). This epidote occurs together with albite in a strongly reacted (complete chloritization of biotite) sample from Valberg and is associated with a development of pores with a diameter on the order of $100\ \mu\text{m}$ (Figure 7e). Some of the albite, which contains inclusions of chlorite schlieren, has a subhedral shape (Figure 7e).

7 | COMPOSITION OF THE LOW-GRADE MINERALS

7.1 | Prehnite

Prehnite is a hydrous calcium aluminium silicate with the formula, $\text{Ca}_2(\text{Al}, \text{Fe}^{3+})_2\text{Si}_3\text{O}_{10}(\text{OH})_2$. According to Deer et al. (2013), the substitution of Al by Fe^{3+} is limited with a $\text{Fe}/(\text{Fe} + \text{Al})$ ratio of up to approximately 0.32. The prehnite analysed in this study (Table S1) is similar in chemical composition with only minor fluctuations. The only considerable variation is Fe and Al (Figure 8). The oxide FeO ranges from 0.15 wt% to 2.49 wt%. One sample with prehnite (MV13.27) stands out with an FeO-content as high as 6.53–8.08 wt%. This corresponds to a $\text{Fe}/(\text{Fe} + \text{Al})$ ratio of 0.19–0.24. There is no clear correlation between Fe content and sample localities. There is however a definite difference in Fe-content between the Fe-rich prehnite in sample MV13.27 and the other samples: The prehnite in this sample is the only prehnite with a euhedral shape.

7.2 | Pumpellyite

The pumpellyite is hydrous calcium aluminium silicate with the general formula $\text{Ca}_2 \text{X} \text{Y}_2(\text{Si}_2\text{O}_7)(\text{SiO}_4)(\text{OH})$,

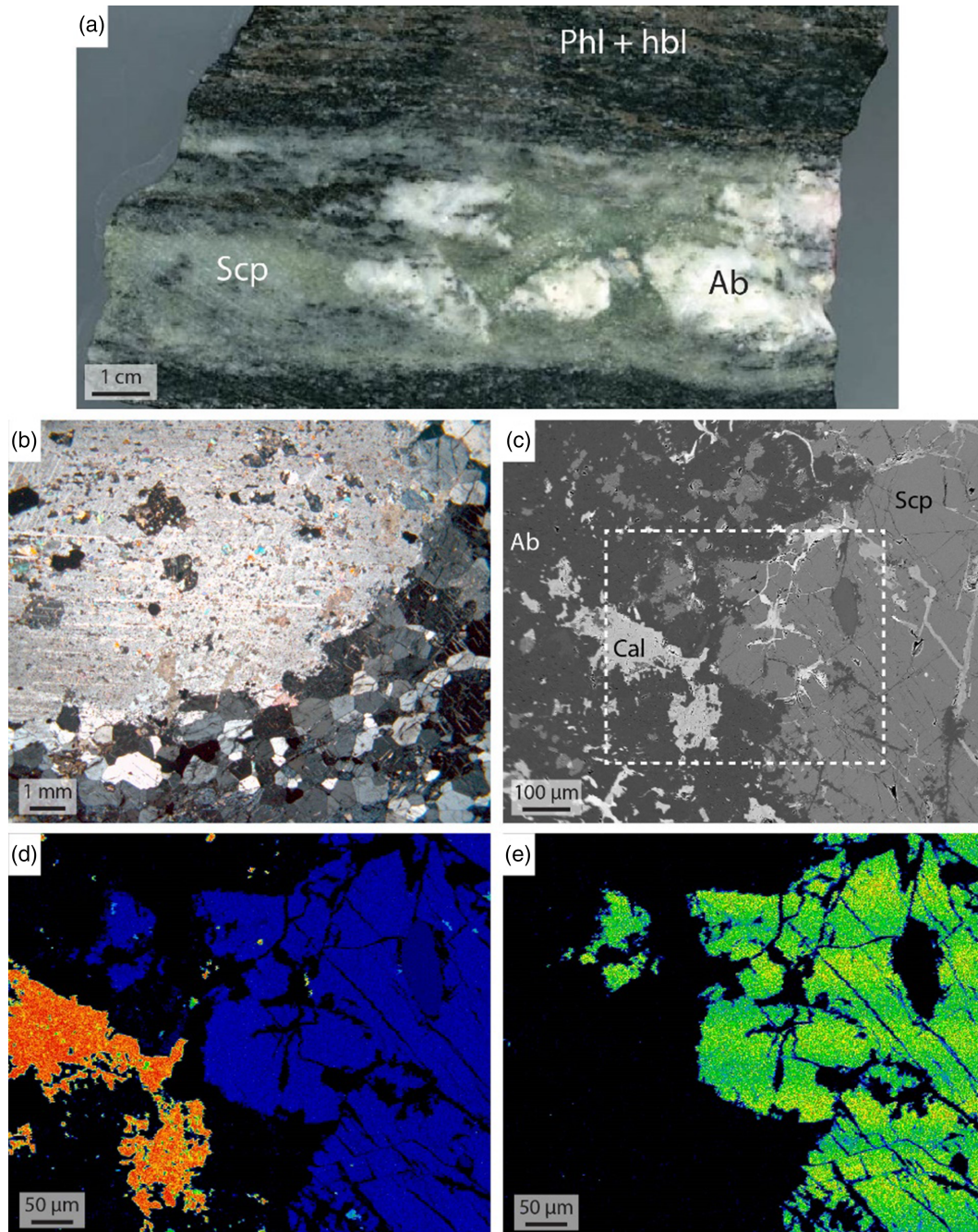


FIGURE 5 Growth of albite porphyroblasts in scapolite-rich metagabbro. (a) Slab of deformed and metasomatised gabbro from Valberg quarry (sample BAM2-12). Dark layers of phlogopite (Phl) and hornblende (Hbl) with a central layer of scapolite (Scp) with porphyroblasts of albite (Ab). (b) Photomicrograph showing a cm large grain of albite with numerous inclusions of calcite, sericite and chlorite. The bottom right part of the image consists of scapolite with minor amphibole. Note that the albite grain replaces a number of small scapolite grains with different crystallographic orientations. (c) BSE image showing the contact between albite with inclusion of calcite (Cal) and scapolite. The stippled white box gives the location of (d) and (e). (d) Element distribution map for Ca over the area outlined by the box in (c). Low Ca in the porphyroblast is in accordance with an albitic composition. (e) Element distribution map for Cl across the same area as in (d) highlighting the location of the scapolite

$O)_2 \cdot H_2O$ where $X = Mg, Fe^{2+}, Mn^{2+}, Fe^{3+}, Al$ and $Y = Al, Fe^{3+}, Mn^{3+}, V^{3+}$. Mg, Fe and Al can vary considerably (Deer et al., 2013; Trzcinski & Birkett, 1982). Depending on the element in the X and Y position,

the pumpellyite group is divided into several species. When iron is the dominant element in both the X and Y positions (>50%) the species is called julgoldite (More, 1971). If Al is dominant in Y position the

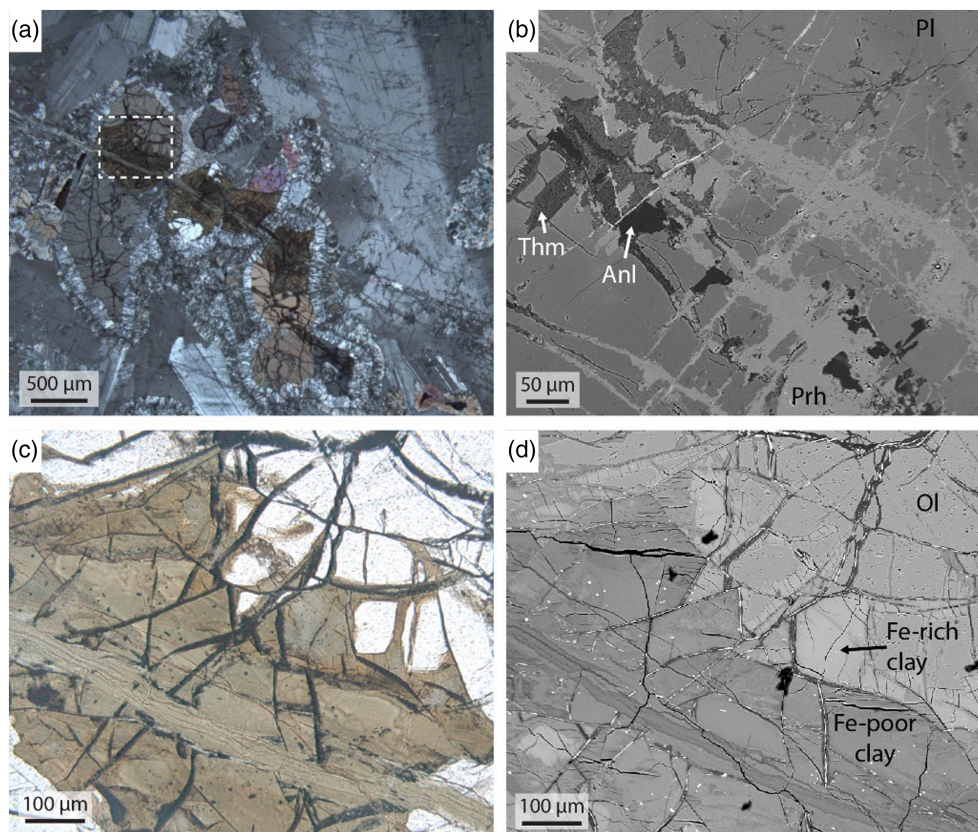


FIGURE 6 Low-grade alteration of coronitic gabbro along microfractures, sample Val-Gp4-1, Valberg quarry. (a) Microphotograph (crossed-polarized light) showing a micro-fracture (upper left to lower right corner) cutting coronitic troctolite and resulting in low-grade alteration of the gabbro. The white stippled box shows the location of (c) and (d). The fracture can be traced from the plagioclase (b) domain through olivine grains (c, d). (b) BSE image showing alteration of the plagioclase domain. The fracture fill consists of analcime (Anl), prehnite (Prh) and thomsonite (Tms). Note that the prehnite also forms away from the main fracture. (c) Microphotograph (plane-polarized light) showing alteration of the olivine along the same fracture. The products are an olive green (closest to the vein) to brown (close to the relic olivine) clay phase. (d) BSE image of the same area as in (c), showing the compositional contrast between the clay phases. A bright phase (high Fe) is developed close to relict olivine and a lower Fe phase is present in adjacent to the centre of the fracture.

species is pumpellyite and depending on the element in the in the X position the pumpellyite is referred to as pumpellyite (Mg), pumpellyite (Fe^{2+}), pumpellyite (Mn), pumpellyite (Fe^{3+}) and pumpellyite (Al), respectively. Most of the pumpellyite analysed here (Table S2, Figure 8) is a low iron variety of the pumpellyite series where the Fe-content varies between 1.1 wt% and 5.8 wt% and belong to the pumpellyite (Al) species of the group. Sample JL1 from Jomfruland contains a markedly higher iron content (up to 17.9 wt% FeO).

7.3 | Epidote

The general formula for the epidote group of minerals is $X_2Y_3Z_3(\text{O},\text{OH},\text{F})_{13}$ where $X = \text{Ca}, \text{Mn},$

Fe^{2+} , $Y = \text{Al}, \text{Fe}^{3+}$, and $Z = \text{Si}$. The composition of epidote coexisting with low-grade minerals is listed in Table S3 and displayed in Figure 8. The main variation in epidote composition reflects substitution of Fe^{3+} for Al. The epidote contains minor amounts of Ti, Mg and Mn.

7.4 | Analcime

Analcime, also known as analcite, has the general formula $\text{Na}[\text{AlSi}_2\text{O}_6]\cdot\text{H}_2\text{O}$ and is a member of the zeolite group, but with structural and chemical similarities to feldspathoids. It is a sodium zeolite where Ca can replace Na in some degree with a ratio of one Ca^{2+} for two Na^+ . The Ca-rich variety in the solid-solution series, which is rare, is called wairakite ($\text{CaAl}_2\text{Si}_4\text{O}_{12}\cdot 2\text{H}_2\text{O}$). There can also be minor amounts of K_2O , up to 2%. Some

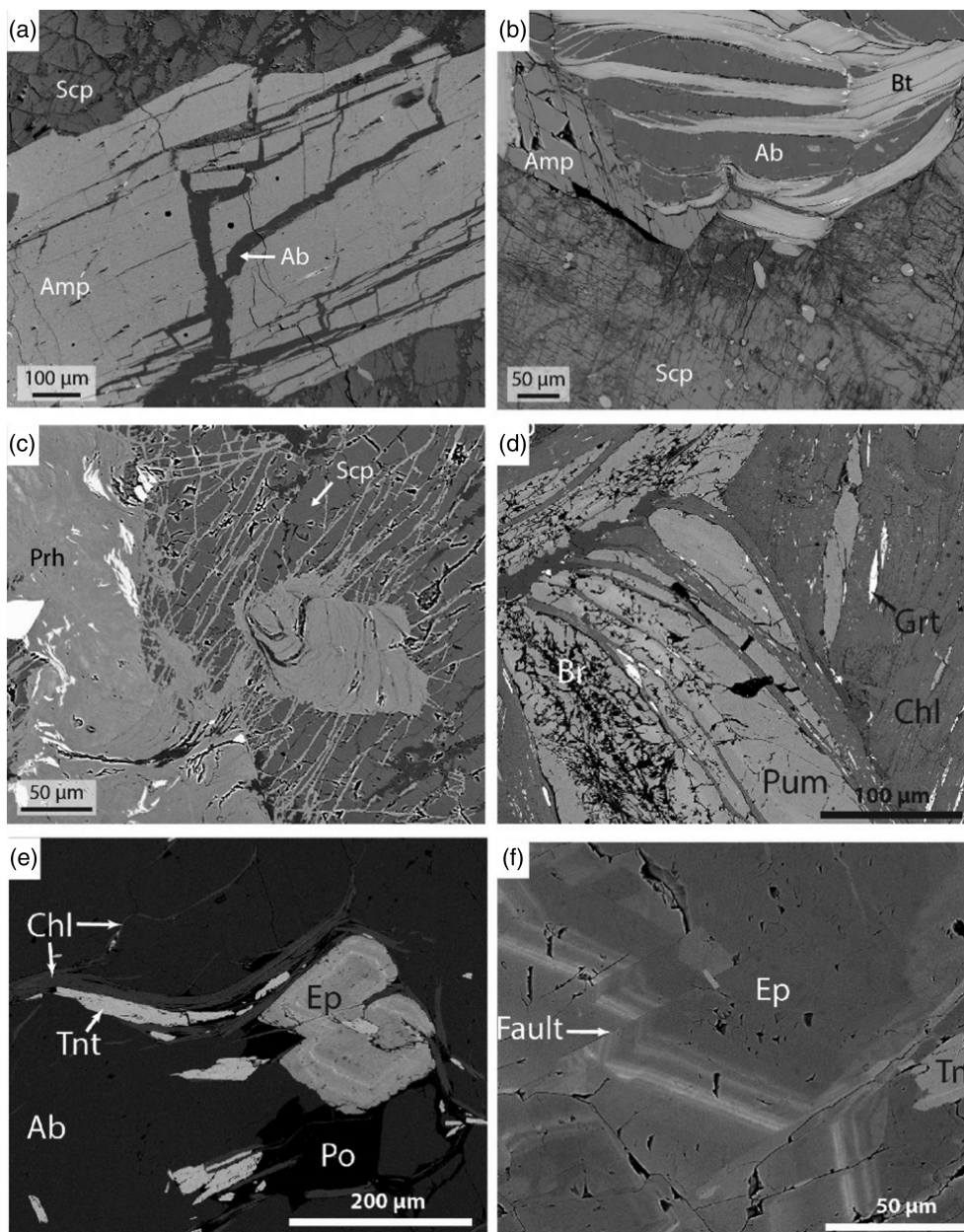


FIGURE 7 Deformation and porosity development associated with displacive growth of low-grade mineral. (BSE images). (a) Albite (Ab) fills the opened cleavage of amphibole (amp). Sample Ri01-09, Ringsjø. (b) Displacive growth of albite between (001) planes of biotite (Bt) leading to strong swelling and bulging of the biotite. The adjacent scapolite grain is fractured and analcime is formed in the high stress points. This implies that the albitization occurred whereas analcime was stable. Sample BAM2-12 from Valberg. (c) Prehnite aggregates surrounded by prehnite-filled fractures in scapolite. Prehnite replaced biotite (no longer present), but there was a displacive element to the reaction as well, evidenced by the fracturing of the surrounding scapolite. Sample AE113, Ringsjø. (d) Brecciation (Br) of the central part of the pumpellyite (Pum), interpreted to represent self-induced deformation of the first formed part of the mineral by growth of the last part or the growth of adjacent grains. Grt: Hydrogarnet, Chl: Chlorite. (e) Pores developed adjacent to oscillatory zoned epidote (ep). Albite with a euhedral shape grows into the pore (bottom right), suggesting that albite grows in the pores (Po) created by the epidote. Note also that the chloritized biotite is bent by the epidote but can locally be followed through the pore. Tnt: Titanite. Sample Val B, Valberg. (f) Displacement of the oscillatory zoning in epidote by micro-faults (arrow). We interpret this faulting to result from forces set up by the growing minerals. Sample Val B, Valberg

substitution occurs between Al^{3+} and Si^{4+} to balance the charge as the water content can vary widely by dehydration/hydration influencing the space available for Na^{+}

and Ca^{2+} (Deer et al., 2013). The compositional variations are affected by the composition of the parent material and the chemical environment (Coombs &

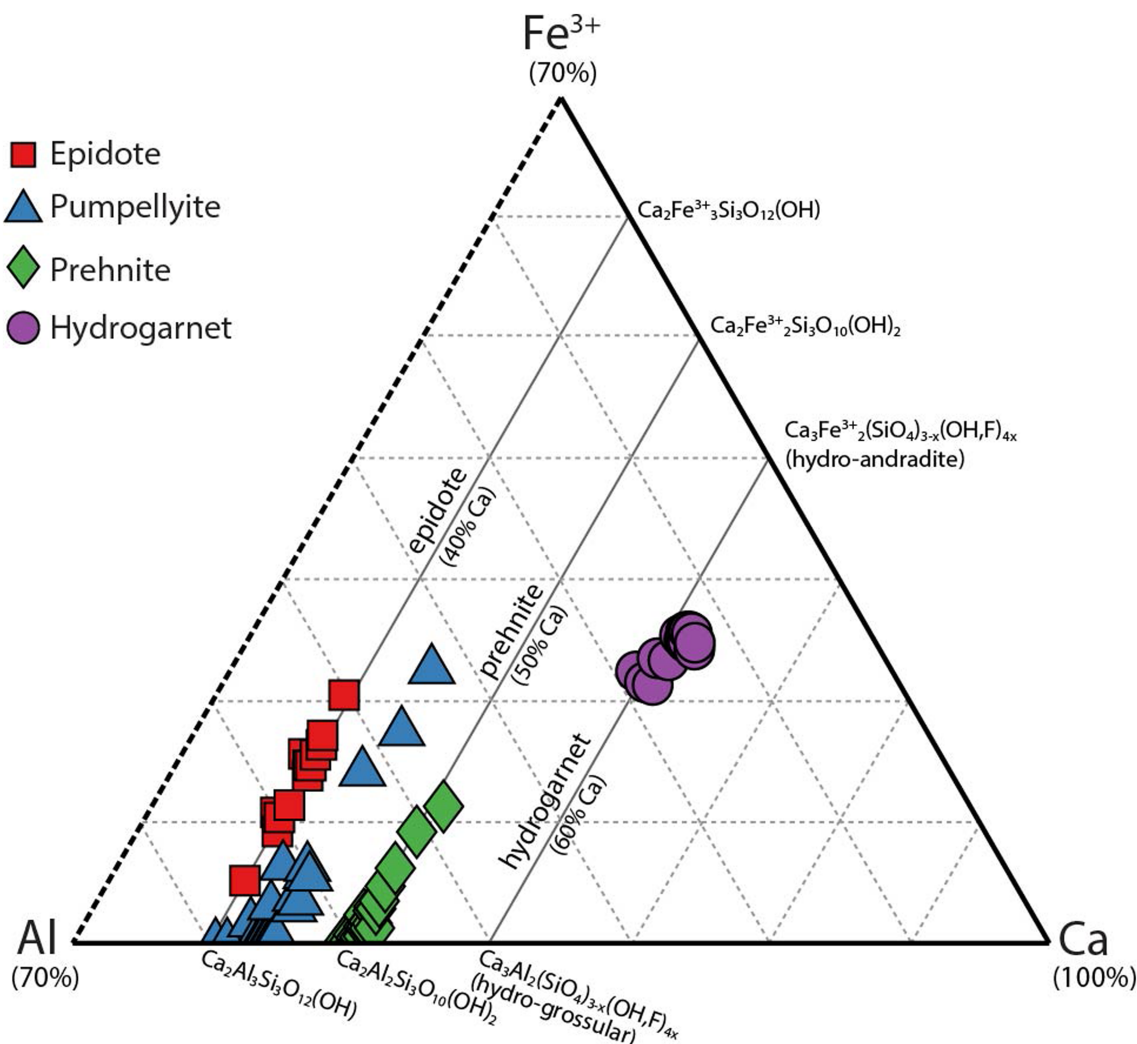


FIGURE 8 Al-Ca-Fe³⁺ diagram showing the compositional variation of prehnite, pumpellyite, hydrogarnet and epidote (in mole proportions)

Whetten, 1967). The compositions of analcime analysed in this work are listed in Table S4. The majority of the analcime is pure Na-analcime with a negligible K and Ca-content. One analcime analysed in sample MV13.35 has a Ca-content of 2.08 wt.%. This analcime is an intermediate mineral in the analcime-wairakite series. The Si:Al ratio of the measured analcime grains ranges from 1.9 to 2.3.

7.5 | Thomsonite

Thomsonite is the name of a series of tectosilicate of the zeolite group ranging from 6NaCa₂Al₅Si₅O₂₀·6H₂O (thomsonite-Ca) to NaSr₂Al₅Si₅O₂₀·6H₂O (thomsonite Sr). The mineral found in sample Val-Gp2-1-14 from the Valberg quarry is the Ca-endmember (Table S5). In addition to thomsonite, Nordrum et al. (2000) reported the zeolites laumonite and heulandite from the same quarry.

7.6 | Hydrogarnet

The general formula of the studied garnet can be written as Ca₃(Al, Fe³⁺, V³⁺, Ti)₂(SiO₄)_{3-x}(OH, F)_{4x} (Figure 8, Table S6). The garnet contains a small amount of goldmanite component with up to 0.5 wt% V₂O₃ (Table S5) and TiO₂ is present in moderate amount highest (up to 1.9 wt% TiO₂) in sample JL1 from Jomfruland. F is moderate (up to 1.3 wt%) and the low total suggests that water together with F substitute at the Si position according to the equation (SiO₄)⁴⁻ ↔ ((OH, F)₄)⁴⁻.

7.7 | Clay-phases after olivine

The two clay phases display distinct composition with respect to MgO (Table S7). The brown clay phases have a low MgO content between 2 and 3 wt.% comparable with ferroan saponite whereas the green phase contains more

MgO of ca. 17 wt%. Both the green and the brown alteration products contain less Mg than the olivine they form from.

7.8 | Kaolinite

Kaolinite ($\text{Al}_2\text{Si}_2\text{O}_5(\text{OH})_4$) is a clay mineral that has been described as an alteration product also from the felsic igneous rocks of the Oslo rift (Trønnes & Brandon, 1992). Kaolinite is present as veins through quartz grains in the nodular gneiss at Valle. As in most cases (Deer et al., 2013), its composition (Table S8) is close to the endmember kaolinite.

8 | METAMORPHIC CONDITIONS

No systematic change in assemblages and mineral chemistry (see above) has been detected across the studied area. The distance between sample JF4 from Jomfruland and Kil is ca. 20 km perpendicular to the contact of the Rift and they both consists of prehnite, pumpellyite and hydrogarnet, typically forming in biotite. Because the low-grade minerals form along veins and are in disequilibrium with the host rock, a meaningful pseudosection approach based on the whole rock composition is not possible. Therefore, we focus on the general stability of the involved low-grade minerals. Figure 9 shows the stability fields of the low-grade minerals prehnite, pumpellyite and analcime as calculated by PerpleX. At a pressure of 1 kbar, the presence of pumpellyite constrains the temperature to be between 75 and 210°C at $X_{\text{H}_2\text{O}} = 1$. Prehnite and analcime are stable to higher temperatures (ca. 400°C) at these pressures and fluid conditions. These estimates are clearly approximations because the minerals are not pure endmembers, and we do not allow for reactions which will lower the stability fields of the various phases shown on Figure 9. Furthermore, the low-grade minerals break down by dehydration reactions, which means that their upper stability temperature will be reduced if the fluid contains CO_2 . As shown in Figure 9, the upper stability field of analcime at 1 kbar is reduced by ca. 50°C if the fluid contains 25% of CO_2 . The stability field of prehnite narrows at increasing pressures, and this mineral becomes unstable at ca. 5 kbar.

Several authors have suggested that $\text{Fe}/(\text{Fe} + \text{Al})$ of pumpellyite decreases with increasing metamorphic grade (Deer et al., 2013; Terbayashi, 1988). The fact that most pumpellyite from the studied area is very low in iron suggests a temperature and pressure in the higher end of the prehnite-pumpellyite facies.

9 | AGE OF THE LOW-GRADE METAMORPHISM

Sample MV13.35, which was used for Ar-dating, is an altered gabbro from the outcrop at Kil brygge, Sannindal, located in the western part of the investigated area around Kragerø. Even though this sample is one of our westernmost samples (with largest distance to the Oslo rift), it still has developed abundant low-grade minerals. The pre-low-grade mineralogy consists of scapolite, amphibole, biotite and plagioclase. K-feldspar forms swelling textures in biotite together with the typical low-grade minerals prehnite and pumpellyite (Figures 3f and S1). It is therefore interpreted to be part of the low-grade assemblage and was used for Ar-Ar dating. The biotite in the same sample is partly altered to chlorite. The chloritization may have provided the potassium required to form K-feldspar. The gabbro is also transected by a number of fractures with extensive albitization.

The K-feldspar from sample MV13.35 defines a spectrum with a flat part (steps 6–12), comprising 41.88% of the total cumulative ^{39}Ar (Figure 10). From these steps, we calculate an inverse weighted mean age of 265.2 ± 0.4 Ma (MSWD = 0.514 and $P = 0.766$) (Table 3, see also Table S9), which we interpret to represent the best estimate of the age of the low-grade metamorphism in the region. The inverse isochron age (263.56 ± 12.33 Ma) overlaps and supports the aforementioned spectrum age; however, the intercept for the trapped air component gives a poor estimate (344.9 ± 274.1 Ma) due to a high portion of radiogenic Ar of the total ^{40}Ar from these heating steps and therefore defines a low spread on the inverse isochron line (2.7%).

10 | DISCUSSION

10.1 | Timing of the low-grade metamorphism and metasomatism

The formation of both the scapolite-metagabbros and the large albitites bodies in the Bamble and Kongsberg lithotectonic domains have traditionally been considered to Sveconorwegian (Meso- to Neoproterozoic) in age (Engvik et al., 2014, 2017; Nijland et al., 2014). In our samples from the Kragerø area, however, the low-grade mineralogy (including albite) is superimposed on previously metamorphosed gabbro and has been dated to be Permian (265.2 ± 0.4 Ma). This suggests that initial, Sveconorwegian amphibolite facies metamorphism led to the formation of amphibole, phlogopite (biotite) and scapolite (Engvik et al., 2011). Later, biotite was the locus of displacive growth of low-grade minerals (see

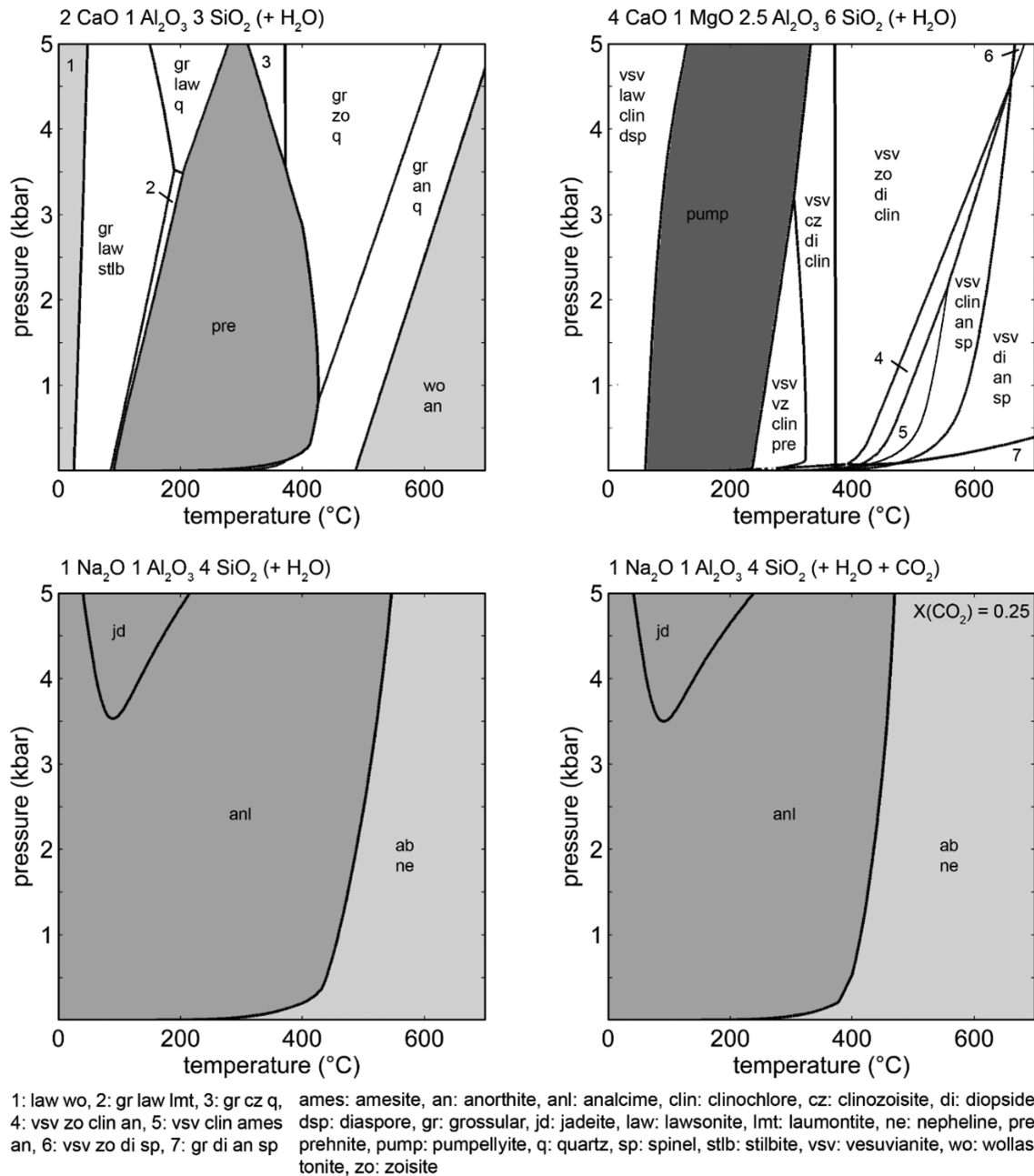


FIGURE 9 Pressure–temperature pseudosections calculated for the ideal composition of prehnite (top left), pumpellyite (top right), and analcime (bottom). The bottom right panel shows how a CO_2 content of the fluid lowers the dehydration temperature of analcime. The stability field of indicator minerals (prehnite, pumpellyite and analcime) were calculated with PerpleX under saturated fluid (pure H_2O , and $\text{H}_2\text{O}/\text{CO}_2$) conditions.

Section 6.1), and biotite, amphibole, and scapolite were replaced by low-grade minerals (see Section 6.2). Two questions have to be addressed: (1) Does the Permian age indeed date the low-grade metamorphism? (2) What is the relation between the albite analysed here and the larger albitites bodies of the area, which have previously been dated to be Sveconorwegian?

1. The Ar–Ar data from K-feldspar (see Section 9) suggest that the low-grade metamorphism is Permian

(265.2 ± 0.4 Ma). There is no reason to interpret this age as a cooling age because the area must have been in a near surface position and cooled below the Ar blocking temperature before the Permian. Additionally, hornblende $^{40}\text{Ar}/^{39}\text{Ar}$ ages between 1090 and 1080 Ma (Cosca et al., 1998) from the Bamble sector record Sveconorwegian hornblende formation. If the K-Feldspar Ar–Ar had been reset during the Permian (instead of recording the first growth of K-Feldspar), this should have been the case for the hornblende as

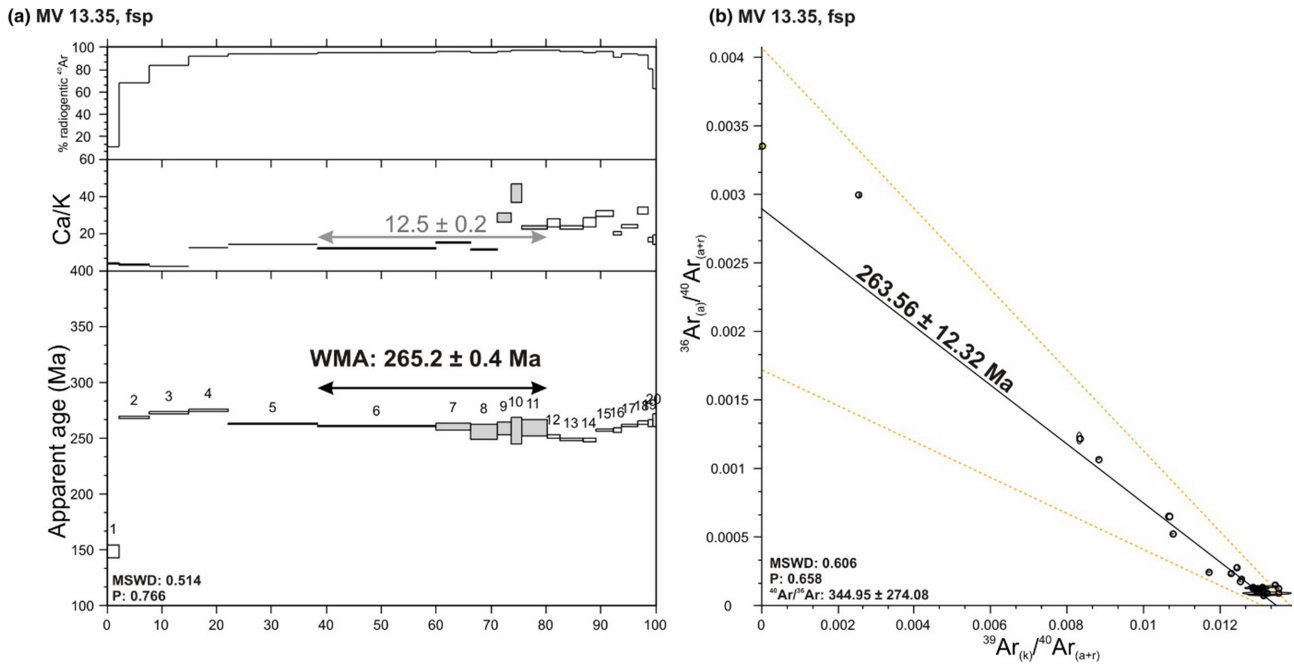


FIGURE 10 Degassing spectrum (a) and inverse isochron result (b) for sample MV 13.35. Terms MSWD, P and WMPA denote mean squared weighted deviance, probability of fit and weighted mean plateau age, respectively. The K/Ca ratios (a) are calculated as $^{39}\text{Ar}/^{37}\text{Ar}$.

well. Nijland et al. (1993) describe low-grade minerals and textures similar to those reported here (K-Feldspar and prehnite lenses along cleavage planes of biotite) from the Froland area. These authors interpreted the low-grade metamorphism to be a retrogressive event following the Sveconorwegian high-grade metamorphism. Based on fission-track ages Nijland et al. (1993) indicated that the low-grade minerals equilibrated between 760 and 920 Ma. Our interpretation, that the dated K-feldspar and associated low-grade minerals grew in Permian time imply that the low-grade metamorphism represent a separate metamorphic event unrelated to the high-grade Precambrian event. Hydrothermal calcite veins with prehnite, albite and the zeolite laumontite from the Kragerø area were dated to be Sveconorwegian (Dahlgren et al., 1993) and interpreted to have formed from hydrothermal solutions, which were exsolved from crystallizing charnockitic intrusions. However, the Sveconorwegian age is based on a Sm-Nd whole rock isochron, so that it is unclear if this indeed dated the low-grade event. Younger ages were proposed by Munz et al. (1995), who describe quartz veins associated with albitization of metagabbros within the Modum complex of the Kongsberg lithotectonic domain that they interpreted to have formed from fluids derived from the overlying sediments in late Precambrian to Permian age. A strong evidence for a Permian age is forward by Sauter et al. (1983) who

reported low-grade minerals (prehnite, pumpellyite and stilpnomelane) from Permian dykes intruding the Bamble lithotectonic domain.

2. Several pieces of evidence suggest that albite is part of the low-grade assemblage in the analysed rocks:

- Where the biotite that is being displaced by albite is surrounded by scapolite, the scapolite shows an increased fracture density around the biotite (Figure 7b), indicating that the fractures formed due to swelling caused by albite growth. Along the fractures, scapolite is reacted to analcime and calcite. This shows that albitization happened when analcime was stable.
- Albite commonly occurs together with prehnite (Figure 3e), suggesting that both minerals formed at the same time and that thus albitization occurred at low-grade conditions. Albite also replaces prehnite (Figure 4d). We interpret this as local variations in the fluid composition whereas the albite and classical low-grade minerals formed broadly contemporaneously.

We report on smaller albitite occurrences related to fracture systems, which may be of a different generation than the larger (presumed Sveconorwegian) bodies as described by Engvik et al. (2014) and Nijland et al. (2014). However, depending on the density of the fractures, the described alteration may also form larger bodies, suggesting that at least some of the larger-scale

TABLE 3 Main $^{40}\text{Ar}/^{39}\text{Ar}$ results

| Sample | Material | Steps | Spectrum | | | Inverse Isochron | | | | | |
|---------|------------|---------|--------------------|-------------------------------------|------------|----------------------|-----------------------|----------------------|-------------|---|------------|
| | | | % ^{39}Ar | Age $\pm 1.96\sigma$ | MSWD (P) | TGA $\pm 1.96\sigma$ | K/Ca $\pm 1.96\sigma$ | Age $\pm 1.96\sigma$ | MSWD (P) | Trapped $^{40}\text{Ar}/^{36}\text{Ar}$ | Spread (%) |
| MV13.35 | K-feldspar | 6-11(6) | 41.88 | 265.17 ± 0.44 | 0.51(0.77) | 264.34 ± 0.64 | 12.52 ± 0.18 | 263.56 ± 12.33 | 0.61(0.658) | 344.95 ± 274.08 | 2.7 |

Note: MSWD and P are the mean squared weighted deviations and probability of fit, spread is the spread along the isochron line (Jourdan et al., 2009). Uncertainties are reported as analytical errors at the 1.96 σ level. The numbers in bold represent the age of low-grade metamorphism.

Na-metasomatism may be of Permian age. We also observe that the albite associated with low-grade minerals contains normally and chessboard twinned albite (see Section 5.1), like in the other albitites in the region (Engvik et al., 2014). Nijland et al. (2014) points to the confusing use of the term albitites in the Bamble lithotectonic domain as it includes both metasomatic altered rocks and apparently magmatic pegmatitic albitite. Possibly, those two types of albitites formed at different times.

10.2 | The low-grade metamorphism fuelled by fluid from the magmatic activity in the Oslo rift

The proximity of the low-grade metamorphism to the Oslo rift gives reasons to believe that the low-grade metamorphism is connected to the magmatic activity in the rift at that time. The age determined here for the low-grade metamorphism (265.2 ± 0.4 Ma) fits to the activity of the Oslo rift: Stage 3 out of five stages of the tectonomagmatic history of the Oslo rift as described by Neumann et al. (1992) occurred 295–275 Ma and represents the main rifting period accompanied by volcanism dominated by rhomb porphyry lavas. Stage 4 (275–240 Ma) represents a change of magmatic style from basaltic shield volcanism to central volcanoes of mixed compositions.

As shown in Figure 1 (see Table 1 for references), low-grade metamorphism is widespread around the Oslo rift. The silver mineralization at Kongsberg is most likely the result of Permian fluid activity as well (Bjørlykke et al., 1990). K-Ar age dating of clay minerals associated with the Kongsberg mineralization gave two clusters of ages with the oldest being ca. 265 Ma (Ineson et al., 1975), which is identical to the age of the low-grade metamorphism dated in this work.

Based on the widespread occurrence of low-grade minerals around the Oslo rift, we suggest that the influence of Permian activity in the domains surrounding the Oslo rift is not limited to the many Permian dykes described from the area but includes low-grade metamorphism and metasomatism (including albitization). The fluid may have been derived from the crystallizing igneous bodies and/or from the surrounding sediments that underwent devolatilizations.

10.3 | The character of the low-grade metamorphism

The low-grade minerals form in displacive and replacive reactions relative to their Precambrian host minerals and as vein fill in the same minerals. The relationship

between the low-grade Permian minerals and their Precambrian host are summarized in a paragenetic model (Figure 11). The Oslo rift is known for its contact metamorphic aureoles around igneous bodies made classical through the work of Goldschmidt (1911) and later by Svensen and Jamtveit (1998) and Jamtveit et al. (2016). The classical contact metamorphism happened within the rift, caused by high-temperature intrusions. Here, however, we report on the effect of the magmatic activity associated with rifting on the surrounding basement rocks, several kilometres away from the present day's border of the Oslo rift. In the present case, the temperature at 1 kbar constrained by the presence of pumpellyite (75 and 210°C at $X_{\text{H}_2\text{O}} = 1$) is several hundred degrees lower than the highest temperature obtained during the classical contact metamorphism. We cannot document a temperature gradient decreasing away from the rift. Thus, the low-grade metamorphism reported here is not a contact metamorphism in the classical sense, but an alteration process induced by fluids from the magmatic activity in the rift. This is in line with the realization of Eskola (1939) that low-grade metamorphism is a hydrothermal event. Numerous reports on albitization in low-grade metamorphic terranes (Miron et al., 2012; Schmidt, 1993) suggest that this is a common phenomenon.

The low-grade minerals contain a higher percentage of water than their host rocks. Therefore, fluids were not only important as possible catalysts of the reactions, but as reactants themselves. Because the low-grade minerals formed at a lower temperature than the original

minerals, it is unlikely that the fluid was derived by local dehydration reactions. It must instead have come from large-scale hydrothermal cells driven by the activity in the rift. Dykes from the Oslo rift penetrate ca. 30 km out from the rift (Sauter et al., 1983) and may also have given off fluid to induce the low-grade metamorphism.

We also observe that the low-grade metamorphism is associated with displacive reactions (see Section 10.4), suggesting that low-grade metamorphism is a dynamic, self-enhancing process that can fracture rocks and thereby facilitate further fluid and mass transport. To our knowledge, this aspect has not previously been discussed in relation to low-grade metamorphisms.

10.4 | Fracturing, porosity and fluid transport aided by displacive reactions

Displacive reactions where the (001) plane of biotite is used as a nucleation site for a range of minerals characterizes the low-grade metamorphic reactions in the studied area. In most cases, this result in a bending of the biotite. Such displacive growth of lens-shaped minerals within sheet silicates has been described previously, including kaolinite in muscovite (sandstone: Arostegui et al., 2001), hydrogarnet in biotite (garnet-amphibolite and granitic gneiss: Nijland et al., 1994; andesine-garnet-biotite-cummingtonite-hornblende rocks: Visser, 1993), K-feldspar in biotite (quartzo-feldspathic igneous and metamorphic rocks: Holness, 2003), and Ca-Al silicates (hydrogarnet, prehnite, pumpellyite, epidote and laumontite) in biotite (calc-alkaline plutonic rocks: Freiburger et al., 2001). For possible explanations as to why the low-grade minerals grow on the cleavage planes of sheet silicates, such as the catalytic effect of biotite surfaces, see Nijland et al. (1994) and Freiburger et al. (2001).

Holness (2003) proposes that the lenses grow in dilatant sites during exhumation of crystalline rocks, especially those containing sheet silicates of high aspect ratio, and indicate a significant grain-scale permeability in the shallow crust. Holness (2003) attributes the bending, and occasional fracturing, of biotite to force of crystallization exerted by the growing K-feldspar on the biotite. However, Holness does not report any fracturing of the surrounding minerals. In contrast, we observe fracturing both in neighbouring grains (Figure 7a-c) and the newly formed minerals themselves (Figures 3e and 7d,f). Similarly, displacive growth of calcite in sandstones and calcretes has been observed to cause an 'explosion' of the surrounding minerals (Saigal & Walton, 1988; Watts, 1978). Such reaction-induced fracturing has been discussed in detail for serpentinization and related

| Mineral | Replacement | | Swelling | | Veining |
|----------------|-------------|-----------------|----------|------------------|---------|
| | Parent | Replacive phase | Host | Displacive phase | |
| Plagioclase | ----- | | | | |
| Amphibole | ----- | | | | |
| Scapolite | ----- | | | | |
| Biotite | ----- | | ----- | | |
| Sericite | | ----- | | | |
| Chlorite | | ----- | ----- | | |
| Albite | | ----- | | ----- | |
| Analcime | | ----- | | | ----- |
| Fe-oxide | | | | ----- | |
| Hydrogrossular | | | | ----- | |
| K-feldspar | | | | ----- | |
| Prehnite | | | | ----- | ----- |
| Pumpellyite | | | | ----- | ----- |
| Kaolinite | | | | | ----- |
| Thomsonite | | | | | ----- |

FIGURE 11 Paragenetic model summarizing the relationship between displacive and replacive low-grade Permian minerals and their Precambrian host minerals. Also displayed are the low grade minerals present as vein fills.

reactions, and can involve significant forces. Kelemen and Hirth (2012) calculated that serpentinization at 200°C may exert forces sufficient to fracture rocks down to 10 km depth. The forces reached during the present case of low-grade metamorphism are not quantified. For displacive reactions to occur, the fluid must be supersaturated, with the displacive force depending on the degree of supersaturations (Watts, 1978). A continuous fluid film from which the minerals can grow is necessary as well, which implies that the ambient pressure must be relatively low, otherwise the fluid film would rupture. This means that the displacive reactions are most likely in the upper part of the crust and may explain why such textures are common consequences of lower grade metamorphism (Freiberger et al., 2001; Holness, 2003, Figure 4), in the weathering zone (Wang et al., 1994) and in sedimentary basins (Saigal & Walton, 1988).

The orientation of biotite controls the initial orientation of the swelling forces, so that a rock with a well-developed biotite fabric will expand perpendicular to the foliation. This is easiest when the rocks are in a shallow setting and the foliation is parallel to the surface. In this case, the swelling can effectively lift the surface, and horizontal fractures would be expected, such as at Ringsjø (Figure 2a). At Valberg, we also observe that 100 µm sized pores are developed adjacent to the displacive mineral epidote (Figure 7e) with growth of euhedral albite inside, suggesting that fluid with dissolved material could move through these pores. Such pores are smaller textural analogues to the centimetre to decimetre-sized vugs that develop along the larger fractures at Ringsjø (see Section 4.2) and may support a model where the larger fractures were opened due to the displacive reactions in favourable situations either close to the surface or where orientation of the biotite was favourable. It is conceivable that such a process might allow fluid to move many kilometres out from the rift zone. This is aided by the porosity development typical for replacement reactions are characterized by the formation of micro-porosity in the replaced phase (Putnis, 2002). Engvik et al. (2009) observed that the albitization in the area is associated with formation of microporosity, and we similarly observe that the reaction products are often porous (Figure 4a,b). Such porosity may also be efficient to transport fluid and may work in tandem with porosity and fractures induced by the displacive reactions.

10.5 | Tectonic consequences

The lifting of the surface, which the displacive growth of low-grade minerals may cause (see Section 10.4),

could have far-reaching consequences. Shoulders that extend 100 to 150 km out from the main rift zone characterize continental rift zones (Sengør 1989). Such rift shoulders are often observed to be uplifted as much as a kilometre or more (Buck, 1986). Uplift of areas adjacent to rifted crust is not predicted by models for stretching and has been explained by convection induced by large horizontal temperature gradients in the mantle (Buck, 1983). On a local scale, the growth of the albite and the other low-grade minerals in biotite results in volume increases of several 100% (Table 2). This poses the question whether the volume increase during low-grade metamorphism and associated metasomatism (albitization) can be responsible for the formation of rift shoulders. If so, it is important to consider that the formation of the albitites through a Permian fluid process as suggested here implies a large-scale mass flux from the rift into the surrounding basement. This may require a revision of tectonic models where constant mass is typically assumed.

11 | CONCLUSIONS

Low-grade metamorphic minerals including prehnite, pumpellyite and analcime are reported from Kragerø area in the classical high grade metamorphic Bamble Sector, South-East Norway.

The low-grade minerals typically form as lenses in biotite together with a range of minerals including albite, K-feldspar and hydrogarnet also interpreted to have formed at low-grade metamorphic conditions.

The growth of the low-grade minerals occurs through displacive reactions that results in swelling of the biotite with fracturing and development of pores adjacent to the swelling textures.

Larger fractures (tenths of meter long) with meter wide alteration selvages with low-grade minerals may also have opened due to displacive reactions. Such fracture channelized fluid and material over minimum distances of 100 ms.

Ar dating of K-feldspar in textural equilibrium with the low-grade minerals yields a Permian age of 256 Ma suggesting that the low-grade metamorphism and parts of the metasomatism induced by fluids from the adjacent Permian Oslo rift.

The low-grade minerals are present adjacent to the Oslo rift, both on its northern and eastern sides in what was the previous shoulder of the rift zone. We speculate that the low-grade metamorphism and metasomatism may have played an active role in uplift required to form shoulders on continental rift zones.

ACKNOWLEDGMENTS


We are grateful to the many students attending the petrology course Geo4860 during the years 2012–2016 for providing some of the data presented in this paper. Christof Kusebauch and Bjørn Jamtveit kindly provided sample BAM2-12 and sample BG94 1A, respectively. We thank Muriel Erambert for help with the probe work and Greg Saunders for developing the Matlab code used to estimate the modal composition of albite and biotite presented in Table 2. Jennifer Porter and Niels Warnecke kindly helped with the many illustrations. H. A. acknowledge a Humboldt prize from the Alexander von Humboldt-Stiftung. We thank an anonymous reviewer and Editor Katy Evans for their helpful comments.

DATA AVAILABILITY STATEMENT

The data that supports the findings of this study are available in the supplementary material of this article.

ORCID

Ane K. Engvik  <https://orcid.org/0000-0002-4530-1646>

Kristina G. Dunkel  <https://orcid.org/0000-0002-4100-381X>

REFERENCES

- Alonso-Azcarate, J., Rodas, M., Bottrell, S. H., Velasco, F., & Mas, J. R. (1999). Pathways and distances of fluid flow during low-grade metamorphism: Evidence from pyrite deposits of Cameros Basin, Spain. *Journal of Metamorphic Geology*, *17*, 339–348. <https://doi.org/10.1046/j.1525-1314.1999.00202.x>
- Andersen, T. (2005). Terrane analysis, regional nomenclature and crustal evolution in the southwest Scandinavian domain of the Fennoscandian shield. *Geologiska Föreningens I Stockholm Förhandlingar*, *127*, 159–168. <https://doi.org/10.1080/11035890501272159>
- Arostegui, J., Irabien, M. J. N., Sanguesa, J., & Zuluaga, M. C. (2001). Microtextures and the origin of muscovite-kaolinite intergrowth in sandstones of the Utrillas formation, Basque Cantabrian Basin, Spain. *Clays and Clays Minerals*, *49*, 529–539. <https://doi.org/10.1346/CCMN.2001.0490605>
- Austrheim, H., Putnis, C. V., Engvik, A. K., & Putnis, A. (2008). Zircon coronas around Fe-Ti oxides: A physical reference frame for metamorphic and metasomatic reactions. *Contributions to Mineralogy and Petrology*, *156*, 517–527. <https://doi.org/10.1007/s00410-008-0299-8>
- Bingen, B., Nordgulen, Ø., & Viola, G. (2008). A four-phase model for the Sveconorwegian orogeny, SW Scandinavia. *Norwegian Journal of Geology*, *88*, 43–72.
- Bingen, B., Skår, Ø., Marker, M., Sigmond, E. M. O., Nordgulen, Ø., Ragnhildstveit, J., Mansfeld, J., Tucker, R. D., & Liegois, J. P. (2005). Timing of continental building in the Sveconorwegian orogeny. *Norwegian Journal of Geology*, *85*, 87–116.
- Bjørlykke, A., Ihlen, P. M., & Olerud, S. (1990). Metallogeny and lead isotope data from the Oslo Paleorift. *Tectonophysics*, *178*, 109–126. [https://doi.org/10.1016/0040-1951\(90\)90462-H](https://doi.org/10.1016/0040-1951(90)90462-H)
- Boles, J. R. (1982). Active albitization of plagioclase, Gulf Coast tertiary. *American Journal of Science*, *282*, 165–180. <https://doi.org/10.2475/ajs.282.2.165>
- Brögger, W. C. (1935). On several Archean rocks from the south coast of Norway. II the south Norwegian hyperites and their metamorphism. *Det Norske Vitenskaps Selskap I Oslo skrifter. Matematisk-Naturvitenskapelig Klasse*, *8*, 1–421.
- Buck, W. R. (1983). Convection beneath continental rifts: The effect on cooling and subsidence, (abstract). *Eos*, *64*, 838.
- Buck, W. R. (1986). Small-scale convection induced by passive rifting: The cause for uplift of rift shoulders. *Earth and Planetary Science Letter*, *77*, 362–372. [https://doi.org/10.1016/0012-821X\(86\)90146-9](https://doi.org/10.1016/0012-821X(86)90146-9)
- Bugge, A. (1936). Kongsberg-Bamble formasjonen. *Norges Geologiske Undersøkelse Bulletin*, *146*. PMID: 117 pp.
- Connolly, J. A. D. (2005). Computation of phase equilibria by linear programming: A tool for geodynamic modeling and its application to subduction zone decarbonation. *Earth and Planetary Science Letters*, *236*, 524–541. <https://doi.org/10.1016/j.epsl.2005.04.033>
- Coombs, D. S. (1954). The nature and alteration of some Triassic sediments from Southland, New Zealand. *Royal Society new Zealand Transactions*, *82*, 65–109.
- Coombs, D. S. (1960). Lower-grade mineral facies in New Zealand. *21st International Geological Congress* (pp. 339–351). Copenhagen.
- Coombs, D. S., Ellis, A. J., Fyfe, W. S., & Taylor, A. M. (1959). The zeolite facies, with comments on the interpretation of hydrothermal syntheses. *Geochimica et Cosmochimica Acta*, *17*, 53–107. [https://doi.org/10.1016/0016-7037\(59\)90079-1](https://doi.org/10.1016/0016-7037(59)90079-1)
- Coombs, D. S., Nakamura, Y., & Vuagnat, M. (1976). Pumpellyite-Actinolite facies schists of the Taveyanne formation near Loèche, Valais, Switzerland. *Journal of Petrology*, *17*, 440–471. <https://doi.org/10.1093/petrology/17.4.440>
- Coombs, D. S., & Whetten, J. T. (1967). Composition of Analcime from sedimentary and burial metamorphic rocks. *Geological Society of America Bulletin*, *78*, 269–282. [https://doi.org/10.1130/0016-7606\(1967\)78\[269:COAFSA\]2.0.CO;2](https://doi.org/10.1130/0016-7606(1967)78[269:COAFSA]2.0.CO;2)
- Cosca, M. A., Metzger, K., & Essene, E. J. (1998). The Baltica-Laurentia connection: Sveconorwegian (grenvillian) metamorphism, veiling, and unroofing in the Bamble sector, Norway. *The Journal of Geology*, *106*, 539–552. <https://doi.org/10.1086/516040>
- Dahlgren, S., Bogoch, R., Magaritz, M., & Michard, A. (1993). Hydrothermal dolomite marbles associated with charnockite magmatism in the Proterozoic Bamble Shear Belt, South Norway. *Contributions to Mineralogy and Petrology*, *113*, 394–409. <https://doi.org/10.1007/BF00286930>
- Deer, W. A., Howie, R. A., & Zussman, J. (2013). *An introduction to the rock-forming minerals*. The Mineralogical Society. <https://doi.org/10.1180/DHZ>
- Engvik, A. K., & Austrheim, H. (2010). Formation of sapphirine during replacement of plagioclase by scapolite in gabbro undergoing mg metasomatism. *Terra Nova*, *22*, 166–171. <https://doi.org/10.1111/j.1365-3121.2010.00929.x>
- Engvik, A. K., Bingen, B., & Solli, A. (2016). Localized occurrences of granulite: P-T modeling, U-Pb geochronology and distribution of early-Sveconorwegian high-grade metamorphism in

- Bamble, South Norway. *Lithos*, 240–243, 84–103. <https://doi.org/10.1016/j.lithos.2015.11.005>
- Engvik, A. K., Corfu, F., Solli, A., & Austrheim, H. (2017). Sequence and timing of mineral replacement reactions during albitization in the high-grade Bamble lithotectonic domain, S-Norway. *Precambrian Research*, 291, 1–16. <https://doi.org/10.1016/j.precamres.2017.01.010>
- Engvik, A. K., Golla-Schindler, U., Berndt, J., Austrheim, H., & Putnis, A. (2009). Intragranular replacement of chlorapatite by hydroxy-fluor-apatite during metasomatism. *Lithos*, 112, 236–246. <https://doi.org/10.1016/j.lithos.2009.02.005>
- Engvik, A. K., Ihlen, P. M., & Austrheim, H. (2014). Characterization of Na-Metasomatism in the Sveconorwegian Bamble sector of South Norway. *Geoscience Frontier*, 5, 659–672. <https://doi.org/10.1016/j.gsf.2014.03.008>
- Engvik, A. K., Metzger, K., Wortelkamp, S., Bast, R., Corfu, F., Korneliussen, A., Ihlen, P., Bingen, B., & Austrheim, H. (2011). Metasomatism of gabbro – Mineral replacement and element mobilization during the Sveconorwegian metamorphic event. *Journal of Metamorphic Geology*, 29, 399–423. <https://doi.org/10.1111/j.1525-1314.2010.00922.x>
- Engvik, A. K., Putnis, A., Fitz Gerald, J. D., & Austrheim, H. (2008). Albitization of granitic rocks: The mechanism of replacement of oligoclase by albite. *Canadian Mineralogist*, 46, 1401–1415. <https://doi.org/10.3749/canmin.46.6.1401>
- Engvik, A. K., Taubald, S., Solli, A., Grenne, T., & Austrheim, H. (2018). Dynamic metasomatism – Stable isotopes, fluid evolution and deformation of albitite and scapolite metagabbro (Bamble lithotectonic domain, South Norway). *Geofluids*, 2018, 9325809–22. <https://doi.org/10.1155/2018/9325809>
- Eskola, P. (1939). Die metamorphen Gesteine. In T. F. W. Barth, C. W. Correns, & P. Eskola (Eds.), *Die Entstehung der Gesteine* (pp. 263–407). Springer. https://doi.org/10.1007/978-3-642-86244-1_3
- Field, D., & Rodwell, J. R. (1968). The occurrence of prehnite in a biotite in a high grade metamorphic sequence from the South Norway. *Norsk Geologisk Tidsskrift*, 48, 58–61.
- Freiberger, R., Hetch, L., Cuney, M., & Morteani, G. (2001). Secondary ca-Al silicates in plutonic rocks: Implications for their cooling history. *Contributions to Mineralogy and Petrology*, 141, 415–429. <https://doi.org/10.1007/s004100100241>
- Frey, M., & Robinson, D. (2009). *Low-grade metamorphism*. Blackwell.
- Goldschmidt, V. M. (1911). *Die Kontaktmetamorphose im Kristianiagebiet* (p. 11). Det Norske Vitenskaps Selskap I Oslo skrifter.
- Kelemen, P. B., & Hirth, G. (2012). Reaction-driven cracking during retrograde metamorphism: Olivine hydration and carbonation. *Earth and Planetary Science Letters*, 345–348, 81–89. <https://doi.org/10.1016/j.epsl.2012.06.018>
- Holland, T. J. B., & Powell, R. (1998). An internally consistent thermodynamic data set for phases of petrological interest. *Journal of Metamorphic Geology*, 16, 309–343. <https://doi.org/10.1111/j.1525-1314.1998.00140.x>
- Holness, M. B. (2003). Growth and albitization of K-feldspar in crystalline rocks in the shallow crust: A tracer for fluid circulation during exhumation. *Geofluids*, 3, 89–102. <https://doi.org/10.1046/j.1468-8123.2003.00052.x>
- Hövelmann, J., Austrheim, H., & Putnis, A. (2014). Cordierite formation during the reaction of plagioclase with mg-rich aqueous solution. *Contributions to Mineralogy and Petrology*, 168, 1063. <https://doi.org/10.1007/s00410-014-1063-x>
- Ineson, P. R., Mitchell, J. G., & Vokes, F. M. (1975). K-Ar dating of epigenetic mineral deposits: An investigation of Permian Metallogenic Province of the Oslo region, southern Norway. *Economic Geology*, 70, 1426–1436. <https://doi.org/10.2113/gsecongeo.70.8.1426>
- Jamtveit, B., & Austrheim, H. (2010). Metamorphism: The role of fluids. *Elements*, 6, 153–158. <https://doi.org/10.2113/gselements.6.3.153>
- Jamtveit, B., Austrheim, H., & Putnis, A. (2016). Disequilibrium metamorphism of stressed lithosphere. *Earth-Science Reviews*, 154, 1–13. <https://doi.org/10.1016/j.earscirev.2015.12.002>
- Jourdan, F., Renne, P. R., & Reimold, W. U. (2009). An appraisal of the ages of terrestrial impact structures. *Earth and Planetary Science Letters*, 286, 1–13. <https://doi.org/10.1016/j.epsl.2009.07.009>
- Kamimura, K., Hirajima, T., & Fujimoto, Y. (2012). Finding of prehnite-pumpellyite facies metabasites from the Kurosegawa belt in Yatsushiro area, Kyushu, Japan. *Journal of Mineralogical and Petrological Sciences*, 107, 99–104. <https://doi.org/10.2465/jmps.111020c>
- Kusebauch, C., John, T., Barnes, J. D., Kügel, A., & Austrheim, H. (2015). Halogen element and stable chlorine isotope fractionation caused by fluid-rock interaction (Bamble sector, SE-Norway). *Journal of Petrology*, 56, 299–324. <https://doi.org/10.1093/petrology/egv001>
- Kusebauch, C., John, T., Whitehouse, M. J., & Engvik, A. K. (2015). Apatite as probe for the halogen composition of metamorphic fluids (Bamble sector, SE Norway). *Contributions to Mineralogy and Petrology*, 170, 34. <https://doi.org/10.1007/s00410-015-1188-6>
- Larsen, B.E. (2014). Structural, geophysical and petrological investigations of the Sarasåsen intrusion and host rocks, Sveconorwegian orogeny, southern Norway. Unpubl. Master Thesis, NTNU, 104pp.
- Lee, J. Y., Marti, K., Severinghaus, J. P., Kawamura, K., Yoo, H. S., Lee, J. B., & Kim, J. S. (2006). A redetermination of the isotopic abundances of atmospheric Ar. *Geochimica et Cosmochimica Acta*, 70, 4507–4512. <https://doi.org/10.1016/j.gca.2006.06.1563>
- Lieftink, D. J., Nijland, T. G., & Maijer, C. (1993). Cl-rich scapolite from Ødegårdens Verk, Bamble, Norway. *Norsk Geologisk Tidsskrift*, 73, 55–57.
- Mansurbeg, H., Morad, S., Suwaidi, M. A., Qurtas, S., Tveiten, A. G., Shahrikhizadeh, S., & Harchegani, F. K. (2020). Meteoric-water incursion into marine turbiditic sandstones: Evidence from the Andrew formation (Paleocene), UK central graben, North Sea. *Marine and Petroleum Geology*, 118, 104428. <https://doi.org/10.1016/j.marpetgeo.2020.104428>
- McDougall, I., & Harrison, T. M. (1999). *Geochronology and thermochronology by the ⁴⁰Ar/³⁹Ar method*. Oxford University Press.
- Miron, G. D., Neuhoff, P. S., & Amthamer, G. (2012). Low-temperature hydrothermal mineralization of island-arc volcanics, south Apusenic Mountains, Romania. *Clays and Clay Minerals*, 60, 1–17. <https://doi.org/10.1346/CCMN.2012.0600101>

- Möller, C., & Söderlund, U. (1997). Age constraints on the regional deformation within the eastern segment, S. Sweden: Late Sveconorwegian granite dyke intrusion and metamorphic-deformational relations. *Föreningen I Stockholm Förhandlingar*, 199, 1–12.
- Morad, S., El-Ghali, M. A. K., Caja, M. A., Al-Ramadan, K., & Mansurbeg, H. (2009). Hydrothermal alteration of magmatic titanite: Evidence from Proterozoic granite rocks, southeastern Sweden. *Canadian Mineralogist*, 47, 801–811. <https://doi.org/10.3749/canmin.47.4.801>
- Morad, S., Sirat, M., El-Ghali, M. A. K., & Mansurbeg, H. (2011). Chloritization in Proterozoic granite from the Æspø laboratory, southeastern Sweden: Record of hydrothermal alteration and implication for nuclear waste storage. *Clay Minerals*, 46, 495–513. <https://doi.org/10.1180/claymin.2011.046.3.495>
- More, P. B. (1971). Julgoldite, the Fe^{2+} – Fe^{3+} dominant pumpellyite: A new mineral from Langban, Sweden. *Lithos*, 4, 93–99.
- Munz, I. A., Yardley, B. W. D., Banks, D. A., & Wayne, D. (1995). Deep penetration of sedimentary fluids in basement rocks from southern Norway – Evidence from hydrocarbon and brine inclusions in quartz veins. *Geochimica et Cosmochimica Acta*, 59, 239–254. [https://doi.org/10.1016/0016-7037\(94\)00322-D](https://doi.org/10.1016/0016-7037(94)00322-D)
- Munz, I. A., Yardley, B. W. D., & Glaeson, S. A. (2002). Petroleum infiltration of high-grade basement, South Norway: Pressure – Temperature – Time – composition (P-T-t-X) constraints. *Geofluids*, 2, 41–53. <https://doi.org/10.1046/j.1468-8123.2002.00029.x>
- Neumann, E. R., Olsen, K. H., Baldrige, W. S., & Sundvoll, B. (1992). The Oslo Rift: A Review. *Tectonophysics*, 208, 1–18. [https://doi.org/10.1016/0040-1951\(92\)90333-2](https://doi.org/10.1016/0040-1951(92)90333-2)
- Nijland, T. G., Harlov, D., & Andersen, T. (2014). The Bamble sector, South Norway: A review. *Geoscience Frontiers*, 5, 659–672. <https://doi.org/10.1016/j.gsf.2014.04.008>
- Nijland, T. G., Liauw, F., Visser, D., Majier, C., & Senior, A. (1993). Metamorphic petrology of the Froland corundum-bearing rocks: The cooling and uplift history of the Bamble sector, South Norway. *Norges Geologiske Undersøkelse Bulletin*, 424, 51–63.
- Nijland, T. G., Verschure, R. H., & Majier, C. (1994). Catalytic effect of biotite: Formation of hydrogarnet lenses. *Comptes Rendues de l'Academie Des Sciences Paris*, 318, 501–506.
- Nordrum, F. S., Larsen, A. O., & Austrheim, H. (2000). Ni-co mineralization in the Valberg quarry, Kragerø, South Norway: A progress report. *Norsk Bergverksmuseum Skrift*, 17, 64–70.
- Putnis, A. (2002). Mineral replacement reactions: From macroscopic observations to microscopic mechanisms. *Mineralogical Magazine*, 66, 689–708. <https://doi.org/10.1180/0026461026650056>
- Putnis, A., & Austrheim, H. (2010). Fluid-induced processes: Metasomatism and metamorphism. *Geofluids*, 10, 254–269.
- Renne, P. R., Mundil, R., Balco, G., Min, K. W., & Ludwig, K. R. (2010). Joint determination of K-40 decay constants and Ar-40*/K-40 for the fish canyon sanidine standard, and improved accuracy for Ar-40/Ar-39 geochronology. *Geochimica et Cosmochimica Acta*, 74, 5349–5367. <https://doi.org/10.1016/j.gca.2010.06.017>
- Ro, H. E., Stuevold, L. M., Faleide, J. I., & Myhre, A. M. (1990). Skagerrak graben – The offshore continuation of the Oslo graben. *Tectonophysics*, 178, 1–10. [https://doi.org/10.1016/0040-1951\(90\)90456-I](https://doi.org/10.1016/0040-1951(90)90456-I)
- Saigal, G. C., Morad, S., Bjørlykke, K., Egeberg, P. K., & Aagaard, P. (1988). Diagenetic albitization of detrital K-feldspar in Jurassic, lower cretaceous, and tertiary clastic reservoir rocks from offshore Norway, I. textures and origin. *Journal of Sedimentary Petrology*, 58, 1003–1013.
- Saigal, G. C., & Walton, E. K. (1988). On the occurrence of displacive calcite in lower old red sandstone of Carnoustie, eastern Scotland. *Journal of Sedimentary Petrology*, 58, 131–135.
- Sansone, M. T. C., & Rizzo, G. (2012). Pumpellyite veins in the metadolerite of Frido unit (southern Apennines – Italy). *Periodico di Mineralogica*, 81, 75–92.
- Sauter, P. C. C., Hermans, G. A. E. M., Jansen, J. B. H., Maijer, C., Spits, P., & Wegelin, A. (1983). Polyphase Caledonian metamorphism in the Precambrian basement of Rogaland/Vest-Agder, Southwest Norway. *Norges Geologiske Undersøkelse*, 380, 7–22.
- Schmidt, S. T. (1993). Regional and local patterns of low-grade metamorphism in the north shore volcanic group, Minnesota, USA. *Journal of Metamorphic Geology*, 11, 401–414. <https://doi.org/10.1111/j.1525-1314.1993.tb00157.x>
- Spooner, E. T. C., & Fyfe, W. S. (1973). Sub-Sea-floor metamorphism, heat and mass transfer. *Contributions to Mineralogy and Petrology*, 42, 287–304. <https://doi.org/10.1007/BF00372607>
- Svensen, H., & Jamtveit, B. (1998). Contact metamorphism of shales and limestones from the Grua area, the Oslo rift, Norway: A phase-petrological study. *Norwegian Journal of Geology*, 78, 81–98.
- Terbayashi, M. (1988). Actinolite-forming reaction at low pressure and the role of Fe^{2+} -mg substitution. *Contribution to Mineralogy and Petrology*, 100, 268–280. <https://doi.org/10.1007/BF00379738>
- Touret, J. L. R. (1971). Le faciès granulite en Norvège méridionale. I. les Associations minéralogiques. *Lithos*, 4, 239–249. [https://doi.org/10.1016/0024-4937\(71\)90004-1](https://doi.org/10.1016/0024-4937(71)90004-1)
- Trønnes, R. G., & Brandon, A. D. (1992). Mildly peraluminous high-silica granites in the continental rift: The Drammen and Finnemarka batholiths, Oslo rift, Norway. *Contributions to Mineralogy and Petrology*, 109, 275–294. <https://doi.org/10.1007/BF00283318>
- Trzcieski, W. E., & Birkett, T. C. (1982). Compositional variations of pumpellyite along the western margin of the Quebec Appalachians. *Canadian Mineralogist*, 20, 203–209.
- Visser, D. (1993). Fluorine-bearing hydrogarnets from Blengsvatn, Bamble sector, South Norway. *Mineralogy and Petrology*, 47, 209–218. <https://doi.org/10.1007/BF01161568>
- Vogt, J. H. L. (1910). Norges Jernmalforekomster. *Norges Geologiske Undersøkelse*, 51, 162–168.
- Wang, Y., Nahon, D., & Merino, E. (1994). Dynamic model of the genesis of calcretes replacing silicate in semi-arid regions. *Geochimica et Cosmochimica Acta*, 58, 5131–5145. [https://doi.org/10.1016/0016-7037\(94\)90299-2](https://doi.org/10.1016/0016-7037(94)90299-2)
- Watts, N. L. (1978). Displacive calcite: Evidence from recent and ancient calcretes. *Geology*, 6, 699–703. [https://doi.org/10.1130/0091-7613\(1978\)6<699:DCEFRA>2.0.CO;2](https://doi.org/10.1130/0091-7613(1978)6<699:DCEFRA>2.0.CO;2)
- Weisenberg, T., & Bucher, K. (2011). Mass transfer and porosity evolution during low temperature water-rock interaction in

gneisses of the Simano nappe: Arvigo, Val Calanca, Swiss Alps. *Contributions to Mineralogy and Petrology*, 162, 61–81. <https://doi.org/10.1007/s00410-010-0583-2>

- White, A. J. R., LeGras, M., Smith, R. E., & Nadoll, P. (2014). Deformation-driven, regional-scale metasomatism in the Hamersley basin, Western Australia. *Journal of Metamorphic Geology*, 32, 417–433. <https://doi.org/10.1111/jmg.12078>
- Whitney, D. I., & Evans, B. W. (2010). Abbreviations for names of rock-forming minerals. *American Mineralogist*, 95, 185–187. <https://doi.org/10.2138/am.2010.3371>
- Zeck, H. P. (1971). Prehnite-Pumpellyite facies metamorphism in Precambrian basement rocks of S. Sweden. *Contributions to Mineralogy and Petrology*, 32, 307–314. <https://doi.org/10.1007/BF00373348>
- Ziegler, P. A. (1978). North Sea rift and basin development. In I. B. Ramberg & E.-R. Neumann (Eds.), *Tectonics and geophysics of continental rifts* (pp. 249–277). Springer. https://doi.org/10.1007/978-94-009-9806-3_21

SUPPORTING INFORMATION

Additional supporting information can be found online in the Supporting Information section at the end of this article.

Table S1. Composition of prehnite. Total iron given as Fe₂O₃. Structural formulae based on 11 oxygen equivalents, assuming that all Fe is Fe³⁺.

Table S2. Composition of pumpellyite. Total iron given as FeO. Structural formulae are based on 49 oxygen equivalents. Where the number of cations was larger than 32, Fe³⁺ was calculated assuming 32 cations and charge balance.

Table S3. Composition of epidote. Total iron given as FeO. Structural formulae based on 12.5 oxygen equivalents, assuming that all Fe is Fe³⁺.

Table S4. Composition of analcime. Total iron given as FeO. Structural formulae based on 6 oxygens. All Fe is assumed to be Fe³⁺. The grey analyses are questionable because of very low Na content, which may be due to instability of analcime under the electron beam.

Table S5. Composition of thomsonite. Total iron given as FeO. Structural formulae based on 20 oxygens, assuming all Fe to be Fe³⁺.

Table S6. Composition of hydrogarnet. Total Fe is given as Fe₂O₃. The total is corrected for O=F. For the structural formulae, all Fe is assumed to be Fe³⁺. Analyses were normalized to (X + Y) = 5, with X = Ca, Fe²⁺, Mg and Y = Al, V, and Ti. The rightmost analyses are from Visser (1993).

Table S7. Composition of olivine and its alteration products. Total iron given as FeO. Structural formulae based on 4 oxygens for olivine and 11 oxygen equivalents for the clay phase, assuming that all Fe is Fe²⁺.

Table S8. Composition of kaoline. Total iron given as FeO. Structural formulae based on 6 oxygen equivalents, assuming that all Fe is Fe³⁺.

How to cite this article: Austrheim, H., Engvik, A. K., Ganerød, M., Dunkel, K. G., & Velo, M. R. (2022). Low-grade prehnite-pumpellyite facies metamorphism and metasomatism in basement rocks adjacent to the Permian Oslo rift: The importance of displacive reactions. *Journal of Metamorphic Geology*, 40(9), 1467–1492. <https://doi.org/10.1111/jmg.12682>